Title:

Functional assessment of a *kcnb1* knock-out zebrafish to model *KCNB1*-related neurodevelopmental and epileptic disorders

Lauralee Robichon[a,c], Claire Bar[a,b,c], Anca Marian[a,c], Lisa Lehmann[a,c], Solène Renault[a,c], Edor Kabashi[a,c,*], Sorana Ciura[a,c], Rima Nabbout[a,b,c]

Affiliations:

[a] Laboratory of Translational Research for Neurological Disorders, INSERM UMR 1163, Institut des maladies génétiques, Imagine Institute, Université Paris Cité, Paris, France

[b] APHP, Reference center for rare epilepsies, Department of Pediatric Neurology, Hôpital Necker-Enfants Malades, member of EPICARE, Paris, France

[c] Université Paris Cité – Sorbonne Université, Paris, France

Authors e-mail addresses:

lauralee.robichon@institutimagine.org; claire.bar@chu-bordeaux.fr; anca.marian@institutimagine.org; lisa.lehmann@etu.unistra.fr; solene.renault@institutimagine.org; edor.kabashi@institutimagine.org; sorana.ciura@institutimagine.org; rima.nabbout@aphp.fr

Corresponding author *:

Edor KABASHI

Laboratory of Translational Research for Neurological Disorders

Imagine Institute

24 Boulevard du Montparnasse

75015 Paris

France

Email: edor.kabashi@institutimagine.org

Declaration of interest: The authors declare that no conflict of interest exists.

Abstract

KCNB1 encodes the Kv2.1 potassium channel α-subunit. *De novo* pathogenic variants of *KCNB1* with loss-of-function (LOF) properties have been associated with neurodevelopmental and epileptic disorders (DEE) diagnosed in early childhood. The study aims to characterize a knock-out (KO) zebrafish line targeting *kcnb1 (kcnb1*$^{+/-}$ and *kcnb1*$^{-/-}$). We examined the spatial expression of kcnb1, as well as phenotypic behavior, cellular, and electrophysiological activity of fish during early development stages. In wild-type larval zebrafish, kcnb1 was found in various regions of the central nervous system but was undetected in the KO model. Both *kcnb1*$^{+/-}$ and *kcnb1*$^{-/-}$ zebrafish displayed impaired swimming behavior and "epilepsy-like" features that persisted through embryonic and larval development, with variable severity. When exposed to the chemoconvulsant pentylenetetrazol (PTZ), mutant fish showed elevated locomotor activity and epileptiform-like electrographic activity. In addition, PTZ-exposed *kcnb1*$^{-/-}$ larvae exhibited higher bdnf mRNA expression and activated c-Fos positive neurons in the telencephalon. In this KO model, neuronal circuits, muscle fibers and neuromuscular junction organization remained unaffected, including normal AchR cluster distribution, although a decreased AchE mRNA expression was observed. *kcnb1* KO zebrafish develops early DEE-like phenotypes that affects neuronal functions. This study highlights the model's relevance for investigating developmental neuronal signaling pathways in *KCNB1*-related DEEs.

Research organism: zebrafish

Keywords: Developmental and epileptic encephalopathy; developmental encephalopathy; voltage-gated potassium channels; KCNB1; $K_V2.1$; potassium channels; zebrafish; electrophysiology

1. Introduction

KCNB1 encodes the pore-forming α1 subunit of the voltage-gated potassium channel subfamily 2 ($K_v2.1$). $K_v2.1$ is extensively expressed across the central nervous system (CNS), particularly in clusters on neuronal soma, proximal dendrites, and axonal initial segment of neurons (Bishop et al., 2015; Du et al., 1998; Sarmiere et al., 2008; Trimmer, 1991). Responsible for a delayed-rectifier outward potassium current, $K_v2.1$ contributes to membrane repolarization, hyperpolarization, and modulates neuronal excitability through activity-dependent regulation of $K_v2.1$ phosphorylation in diverse neuronal subtypes (Antonucci et al., 2001; Bishop et al., 2015; Du et al., 1998; Mohapatra et al., 2009). Beyond conduction, $K_v2.1$ channels participate in intracellular protein trafficking and calcium signaling (Antonucci et al., 2001; Johnson et al., 2018; Vierra et al., 2019). Pathogenic *KCNB1* variants have been reported in patients with developmental and epileptic encephalopathy (DEE), but also in patients with developmental encephalopathy (DE) with late-onset and pharmacoresponsive epilepsy, or without epilepsy (Bar et al., 2020a; Bar et al., 2020b; de Kovel et al., 2017; Marini et al., 2017). All patients reported in the largest series exhibit poor long-term outcome associated with a wide phenotypic spectrum including severe intellectual disability, attention disorders and autism spectrum disorder (ASD) (Bar et al., 2020a, 2020b, 2022). Truncating variants correlate with a less severe epileptic phenotype compared to individuals with missense variants (Bar et al., 2020b).

KCNB1 variants functionally characterized *in vitro* display varying degrees of loss-of-function (LOF) exhibiting dominant negative effects such as reduced potassium conductance,

altered ion selectivity, and diminished expression and localization of $K_v2.1$ channels at the cell surface (Kang et al., 2019; Saitsu et al., 2015; Thiffault et al., 2015; Torkamani et al., 2014). Rodent models, including *Kcnb1* knock-out (KO) and knock-in (KI) mice, confirmed these findings by revealing altered behavior including locomotor hyperactivity, reduced anxiety-like behavior and lower chemoconvulsant seizure thresholds (Hawkins et al., 2021; Kang et al., 2024; Speca et al., 2014). Spontaneous seizures have been only reported in the homozygous KI *Kcnb1*$^{R/R}$ (*Kcnb1*$^{G379R/G379R}$) (Hawkins et al., 2021) and the KI *Kcnb1*^{R312H} (Bortolami et al., 2022) mouse models. However, the pathogenic pathways underlying *kcnb1* in DEEs (*kcnb1*-DEEs) have not yet been elucidated and rodent models pose limitations hindering rapid drug screening. In the last decade, due to its genetic manipulability, rapid development, and suitability for high-throughput screening, zebrafish have gained prominence in modeling human brain disorders, including epilepsy (Crouzier et al., 2021; Gawel et al., 2020a; Kolesnikova et al., 2022; Sakai et al., 2018; Yaksi et al., 2021). Significantly, zebrafish larvae subjected to pentylenetetrazol (PTZ), a proconvulsant compound, manifest behaviors akin to seizures, rendering them a valuable model for epilepsy investigations (Baraban et al., 2005). Specifically, PTZ elicits seizure-like responses in zebrafish larvae characterized by stereotypical swimming aberrations featuring locomotor hyperactivity (stage I), circular trajectories (stage II), and clonus-like convulsions accompanied by brief loss of posture (stage III), concomitant with epileptiform electrographic patterns in the zebrafish optic tectum (Afrikanova et al., 2013; Baraban et al., 2005). Zebrafish has proven to be an effective in modeling various genetic epilepsies, supporting its relevance in neurodevelopmental disease research. As example, many models were developed for Dravet syndrome related to *SCN1A* (Baraban et al., 2005; Tiraboschi et al., 2020; Zhang et al., 2015), *STXBP1*-DEE (Grone et al., 2016; Suo et al., 2021), for pyridoxine-dependent epilepsy (Pena et al., 2017), *TSC2* model for tuberous sclerosis complex (Scheldeman et al., 2017), *CACNA1A* in absence seizures (Gawel

et al., 2020b) and *DEPDC5* related epilepsies (de Calbiac et al., 2018; Swaminathan et al., 2018). Characterization of epilepsy-like behavior have been possible as early as 28 hours post-fertilization (hpf), when embryos exhibit stereotyped premotor activity, (de Calbiac et al., 2018). In addition, drug screening in zebrafish larvae has been performed using both genetic and chemically induced epilepsy models, demonstrating the translational potential of this model by identifying compounds able of decreasing the severity of epileptic seizures (Afrikanova et al., 2013; Baraban et al., 2013; Ibhazehiebo et al., 2020; Li et al., 2021; Shin et al., 2022; Tiraboschi et al., 2020; Whyte-Fagundes et al., 2024; Winter et al., 2021).

The zebrafish orthologue of *KCNB1, kcnb1,* shares 67% sequence homology with the human gene. *kcnb1* expression increases during zebrafish development, starting at 19 hpf in zebrafish embryos and mainly found in the brain of adult zebrafish, with tissue-specific expression patterns comparable to mammals (Jedrychowska et al., 2021). A first *kcnb1* KO zebrafish model (*kcnb1*$^{-/-}$) was generated using CRISPR/Cas9 site-specific mutagenesis, leading to a premature termination codon between the N-terminal cytoplasmic domain and the first transmembrane domain of the protein (Shen et al., 2016). Phenotypic characterization of this *kcnb1*$^{-/-}$ model revealed small proportion of gastrulation defect and reduced brain ventricles (Shen et al., 2016) along with disruption of the inner ear development (Jedrychowska et al., 2021), emphasizing *kcnb1*'s role in developmental signaling pathways. Survival rate was reduced in *kcnb1*$^{-/-}$ adult zebrafish compared to WT (Jedrychowska et al., 2021). However, the behavioral phenotypes and epilepsy-like behavior remain unexplored in this *kcnb1* KO zebrafish model.

In this study, we characterized the phenotype of developing zebrafish with inactivated K_v2.1 channels, providing insights into key features of *KCNB1*-DEEs at different stages of development.

2. Results

2.1. kcnb1 is expressed in diverse regions of the CNS in Wild-type larval zebrafish

Previous studies demonstrated the large expression of *kcnb1* in eyes, ears and central nervous system of wild-type fish at 72 hpf using whole-mount *in situ* hybridization and antisense Dig-labelled RNA probes against *kcnb1* (Shen et al., 2016) and presents early RNA expression appearance starting from 19 hpf (Jedrychowska et al., 2021). To complete spatial expression of the protein in the brain of zebrafish, we performed immunohistochemistry on brain slices labelling kcnb1 in WT larvae fish at 6 dpf **(Figure 1A-1D)**. The kcnb1 protein is mainly expressed in the Diencephalon region, in the Midbrain region including the optic tectum, and in the Hindbrain region comprising the cerebellum and in the spinal cord **(Figure 1A-1C)**. However, the protein was not found in the Telecephalon and presented low expression in eyes **(Figure 1A, B)**. High magnification could identify the protein at the cell surface, seemingly following the shape of the neuronal soma **(Figure 1D)**. These results indicate similar profile of expression in the CNS of WT larvae fish between the kcnb1 protein and the RNA obtained by Shen et al. (2016) and Jedrychowska et al. (2021).

2.2. Genotypic characterization of a kcnb1 knock-out zebrafish model

The zebrafish genome contains a single *kcnb1* ortholog (ENSDARG00000060095) which shares 67% of nucleotide identity with the human *KCNB1* gene (ENSG00000158445), showing a high degree of conservation. Using a *kcnb1* knock-out zebrafish model generated by Shen et collaborators (2016), obtained by CRISPR/Cas9 genome editing by introducing a premature stop codon in the first exon of the gene, we investigated loss-of-function properties of *kcnb1* in the context of DEEs. After few crosses of $kcnb1^{+/-}$ males and $kcnb1^{+/-}$ females, we obtained a complete *kcnb1* knock-out line which was, in first hand, clearly identifiable by a 2-G bases deletion and an insertion of a 14 bp-nucleotide sequence on chromatograms (Δ14bp) **(Figure 2A)**. We could easily identify a melting curve shift due to DNA mutations in $kcnb1^{+/-}$ and $kcnb1^{-}$

$^{/-}$ adult fish compared with *kcnb1*$^{+/+}$ fish using the HRMA technique **(Figure 2B)**. We noticed significant reduced levels of *kcnb1* expression, normalized according to *actin* mRNA expression, in both *kcnb1*$^{+/-}$ and *kcnb1*$^{-/-}$ zebrafish larvae compared with their WT (*kcnb1*$^{+/+}$ = 1 ± 0 arbitrary unit (AU); *kcnb1*$^{+/-}$ = 0.56 ± 0.096 AU; *kcnb1*$^{-/-}$ = 0.44 ± 0.084 AU; +/+ *vs* mutants: $p<0.01$) **(Figure 2C)** that was confirmed by the absence of the protein expression in the brain of both mutant conditions **(Figure 2D)**. The survival of all tree genotypes (+/+, +/- and -/-) was monitored from 0 to 15 dpf, the critical period of zebrafish development. Both heterozygous and homozygous *kcnb1* zebrafish lines developed normally and the survival at the larval stages was very similar to non-transgenic controls during this period reaching above 80% of living fish at 15 dpf (+/+ *vs* mutants: $p>0.5$) **(Figure 2E, Figure 2-table 2)**. These results indicate that the loss of *kcnb1* do not impact the normal growth of fish at early stages of development.

2.3. Loss of kcnb1 function leads to altered behavior phenotype

Zebrafish embryos exhibit an early stereotyped behavior consisting of alternating spontaneous tail coiling in zebrafish involving side-to-side contractions of the trunk due to synchronized bilateral spinal circuitry (Saint-Amant and Drapeau, 2001). This premotor activity begins at 17 hpf, reaching a peak at 19 hpf, and then decreases gradually until 27 hpf (Saint-Amant and Drapeau, 1998). We assessed a premotor behavior by measuring the spontaneous tail coiling at 26 hpf. Both *kcnb1* mutant zebrafish showed a tail coiling activity decreased by half compared to WT zebrafish (tail coiling number*:* *kcnb1*$^{+/+}$ = 3.21 ± 0.17; *kcnb1*$^{+/-}$ = 1.48 ± 0.098; *kcnb1*$^{-/-}$ = 1.75 ± 0.14; +/+ *vs* mutants: $p<0.001$) **(Figure 3-figure supplement 1, Figure 3-video 1A-C).** Given these results and the known variation in coiling activity with embryos developmental age, we quantified tail coiling from 24 to 36 hpf aiming to determine the time point of appearance of this early phenotype in *kcnb1* mutant embryos. A significant decreased of tail coiling activity was found since 25 hpf in both *kcnb1*$^{+/-}$ and *kcnb1*$^{-}$

$^{/-}$ mutants compared to wild-type embryos (tail coiling number at 25 hpf: *kcnb1*$^{+/+}$ = 2.98 ± 0.20; *kcnb1*$^{+/-}$ = 2.12 ± 0.108; *kcnb1*$^{-/-}$ = 2.07 ± 0.18; +/+ *vs* mutants: p<0.01), persisting until 31 hpf until the period where all conditions were completely inactive (tail coiling number at 31 hpf: *kcnb1*$^{+/+}$ = 0.52 ± 0.83; *kcnb1*$^{+/-}$ = 0.13 ± 0.036; *kcnb1*$^{-/-}$ = 0.14 ± 0.04; +/+ *vs* mutants: p<0.0001) **(Figure 3A, B)**. This suggests these *kcnb1* mutant lines were not capable to perform complex stereotyped behavior.

Starting at 21 hpf, the touch-evoked escape responses (TEER) is characterized by rectilinear swimming away from the stimulus at 48 hpf (Saint-Amant and Drapeau, 1998). Spontaneous and PTZ-induced seizure-like behavior have been previously associated with elevated swim activity and non-rectilinear, "whirlpool-like" circling swim behavior (Baraban et al., 2013, 2005; de Calbiac et al., 2018). We used the TEER to explore early swimming trajectory patterns associated with *kcnb1* loss-of-function in zebrafish larvae. After stimulation by light tail touch, mutant zebrafish exhibited aberrant locomotion characterized by rapid motion circular swimming compared to wild type which showed straight-line trajectories **(Figure 3C, Figure 3-video 2A-B)**. Indeed, the total distance swam, velocity and time spent in motion based on the TEER trajectories were significantly increased in both *kcnb1*$^{+/-}$ and *kcnb1*$^{-/-}$ mutants compared to the WT condition (distance swam: *kcnb1*$^{+/+}$ = 57.75 ± 4.23 mm; *kcnb1*$^{+/-}$ = 100.26 ± 7.13 mm; *kcnb1*$^{-/-}$ = 93.8 ± 7.10 mm; +/+ *vs* mutants: p<0.0001) **(Figure 3D-F)**. Interestingly, we observed a variability in the trajectory of embryo **(Figure 3-table 3**). Within the same condition, embryos were divided into two distinct groups: severe phenotype (SP) for which the inclusion limit was that the fish had to perform a minimum of two swim circles, and mild phenotype (MP) which grouped other trajectories that could be identified **(Figure 3-table 3, Figure 3-figure supplement 2A)**. 30% of *kcnb1*$^{+/-}$ embryos had a severe phenotype versus 52% of *kcnb1*$^{-/-}$ embryos, indicating a large variability in swimming behavior within the same condition **(Figure 3-table 3).** The variability between both swimming phenotypes was

quantified following the same parameters of the TEER test and results show similar values between both mutant conditions presenting a mild phenotype as compared to the control condition (*kcnb1*$^{+/+}$). Nevertheless, fish with a severe phenotype present a significant increase of the studied parameters for both genotypes (*kcnb1*$^{+/-}$ and *kcnb1*$^{-/-}$) (distance swam: p(+/+ *vs* +/- MP)>0.5; p(+/+ *vs* +/- SP)<0.0001; p(+/+ *vs* -/- MP)>0.5; p(+/+ *vs* -/- SP)<0.0001) **(Figure 3-figure supplement 2B)**.

2.4. kcnb1 mutant models displayed light and sound-induced locomotor impairments

Previous studies on zebrafish model of genetic epilepsies reported locomotor changes and seizure-like behavior induced by light stimulus (Pena et al., 2017; Scheldeman et al., 2017; Siekierska et al., 2019). To determine whether the early altered behavioral phenotype associated with *kcnb1* loss-of-function persists in later developmental stages, we assessed spontaneous locomotor activity in zebrafish larvae from 3 to 6 dpf. We examined the responses evoked by light changes in *kcnb1* homozygous and heterozygous mutants from 3 to 6 dpf (light/dark switch). After a 15-min habituation period, each larva was recorded for 60 minutes over three light/dark cycles (each consisting of 10 min in light and 10 min in dark setting per cycle, **Figure 4A-C, Figure 4-video 3).** At 3 and 4 dpf, the three conditions presented global low locomotor activity that was significantly increased for all conditions at later days (+/+ *vs* mutants: p>0.5) **(Figure 4C)**. However, a significant gap was observed starting from 5 dpf with a locomotor hyperactivity for *kcnb1*$^{-/-}$ larvae as compared to WT and *kcnb1*$^{+/-}$ fish, reflecting the result obtained in **Figure 4B** following the described light/dark protocol where *kcnb1*$^{-/-}$ mutants showed significant locomotor hyperactivity induced by light/dark transitions (distance at 6 dpf: *kcnb1*$^{+/+}$ = 3.98 ± 0.43 cm; *kcnb1*$^{+/-}$ = 3.42 ± 0.54 cm; *kcnb1*$^{-/-}$ = 8.29 ± 0.76 cm; +/+ *vs* -/- : p<0.0001). A second protocol following brief and repeated audio stimuli showed significant decrease of the locomotor activity for both mutant models (*kcnb1*$^{+/-}$ and *kcnb1*$^{-/-}$) as compared to the WT condition (+/+ *vs* mutants: p<0.5) **(Figure 4D).** These results seem indicating that

the observed locomotor phenotype could be due to dysregulations of electrical neuronal activity involving different sensorimotor pathways.

2.5. kcnb1 mutants exhibited increased sensitivity to PTZ-induced seizures

Previous studies have demonstrated that exposure of zebrafish larvae to pentylenetetrazol (PTZ) induces increased locomotor activity and seizure-like stereotypic behavior in a concentration-dependent manner (Baraban et al., 2005). The susceptibility of larvae to chemically induced seizures by PTZ was tested in the *kcnb1* LOF model. We analyzed the locomotor activity from 3 to 6 dpf larvae exposed to PTZ at concentration of 5 mM. Consistent with our previous results, the 30 minutes baseline activity of *kcnb1* mutants was similar to that of age-matched wild-type in dark condition **(Figure 5A, B).** At 3 dpf, there was no significant difference in locomotor hyperactivity induced by PTZ exposure between the different conditions **(data not shown).** In contrast, after 30 minutes of PTZ exposure from 4 dpf to 6 dpf, both *kcnb1* mutant models (*kcnb1*$^{+/-}$ and *kcnb1*$^{-/-}$) maintained a significantly higher swimming activity as compared to their control larvae (distance at 60 min: *kcnb1*$^{+/+}$ = 8.59 ± 4.23 cm; *kcnb1*$^{+/-}$ = 40.9 ± 6.86 cm; *kcnb1*$^{-/-}$ = 37.9 ± 5.60 cm; +/+ *vs* mutants: $p<0.0001$), and characterized by fast circles indirectly indicating an increase of induced seizure-susceptibility **(Figure 5A, B)**. To investigate possible molecular disruptions in the *kcnb1* LOF zebrafish model, we quantified the *bdnf* mRNA expression, a neurogenesis and epileptogenesis-related gene, following a similar pre- and post-PTZ treatment as described previously **(Figure 5C)**. During the basal activity of fish, the *kcnb1*$^{-/-}$ condition showed a tendency to an elevated expression of *bdnf* mRNA as compared to both *kcnb1*$^{+/-}$ and WT fish (*kcnb1*$^{+/+}$ = 1 ± 0 AU; *kcnb1*$^{+/-}$ = 2.28 ± 0.42 AU; *kcnb1*$^{-/-}$ = 3.01 ± 0.45 AU; +/+ *vs* mutants: $p>0.5$) **(Figure 5C)**. Indeed, the expression of *bdnf* was significantly increased in *kcnb1*$^{-/-}$ fish treated with PTZ as compared to the WT-treated condition (*kcnb1*$^{+/+}$ = 1.56 ± 0.27 AU; *kcnb1*$^{+/-}$ = 3.24 ± 1.24 AU; *kcnb1*$^{-/-}$ = 29.4 ± 6.99 AU; +/+ *vs* -/-: $p<0.0001$) **(Figure 5C)**. Finally, the acute neuronal

activation was analyzed following the same pre- and post-PTZ treatment in the brain of whole-mounted zebrafish at 6 dpf and immunostained with anti-c-Fos. The telencephalon was the major region activated after the chemical treatment for each genotype **(Figure 5D, Figure 5-figure supplement 3A).** The quantification of fluorescent c-Fos positive neurons normalized to the volume of the telencephalon did not reveal any difference in the number of activated neurons in both mutant conditions (*kcnb1*$^{+/-}$ and *kcnb1*$^{-/-}$) as compared to the WT condition either in pre- or post-PTZ treatment (+/+ *vs* mutants: $p>0.5$) **(Figure 5E).** Based on the similar total number of activated neurons, we analyzed the distribution of neurons according to the fluorescence intensity value of c-Fos in the telencephalon of fish, reflecting the level of neuronal activation that was divided in four equal shares (from 0 to 100%): low (0-25%), moderately low (25-50%), moderately high (50-75%) and high (75-100%) neuronal activation **(Figure 5E, Figure 5-figure supplement 3B).** The three non-treated conditions were presenting a similar distribution with a majority of low neuronal activation of c-Fos positive neurons. However, chemically treated *kcnb1*$^{-/-}$ fish were presenting a global higher activation with a significant shift to a moderately low and moderately high neuronal activation (+/+ *vs* -/- : $p<0.5$) **(Figure 5E, Figure 5-figure supplement 3B).** These results indicate that *kcnb1* LOF model presents neurogenesis impairments in the developmental brain of fish.

2.6. kcnb1 knock-out zebrafish models show increased electrophysiological activity in response to epileptogenic treatment at 5dpf

Abnormal electrographic activity has been demonstrated in chemically provoked-epileptic seizures zebrafish models and were associated with hyperactivity and PTZ hypersensitivity (Afrikanova et al., 2013; Baraban et al., 2005; Shin et al., 2022). To investigate whether *kcnb1* knock-out resulted in abnormal brain activity electrographically, local field potentials (LFPs) were obtained from the optic tectum of agarose-embedded 5 dpf-zebrafish larvae. Neuronal activity of fish was recorded during a “basal activity” phase of 30 minutes, followed by

application of the PTZ treatment. Provoked seizures were recorded for an additional 30 minutes **(Figure 6A).** Control and *kcnb1* knock-out larvae models presented spontaneous neuronal activity bursts representing a summation of synchronized events **(Figure 6B).** We did not find a significantly increased number of spikes in the basal neuronal activity of *kcnb1*$^{+/-}$ and *kcnb1*$^{-/-}$ larvae when compared with WT (*kcnb1*$^{+/+}$ = 171 ± 23.21 spikes; *kcnb1*$^{+/-}$ = 149 ± 49.22 spikes; *kcnb1*$^{-/-}$ = 256 ± 100.8 spikes; +/+ *vs* mutants: $p>0.5$) **(Figure 6C)**. In response to 40 mM PTZ, control larvae presented spikes with a regular frequency associated with an increase in number of spikes in comparison with the same non-treated condition (PTZ-exposed *kcnb1*$^{+/+}$ = 1190 ± 227.4 spikes; +/+ *vs* PTZ-exposed +/+: $p<0.5$). A similar neuronal activity profile, reflected by the count of spikes number, was observed in the *kcnb1*$^{-/-}$ model following the chemical treatment after 10 minutes although presenting polyspike discharges as compared to the WT condition (PTZ-exposed *kcnb1*$^{-/-}$ = 1246 ± 367.7 spikes; -/- *vs* PTZ-exposed -/-: $p<0.5$) **(Figure 6C)**. The lack of significant spike number changes could be linked to insufficient PTZ exposure timing or to variable phenotypes (mild and severe, see **Figure 3-table 3**) as observed for the TEER test. Interestingly, the *kcnb1* heterozygous deletion mutant (*kcnb1*$^{+/-}$) showed a significant higher increase of number of spikes induced by PTZ and exhibited polyspike discharges as compared to the control condition (PTZ-exposed *kcnb1*$^{+/-}$ = 2801 ± 799.5 spikes; +/- *vs* PTZ-exposed +/-: $p<0.01$) **(Figure 6C, Figure 6-table 4).** These results suggest that the loss of *kcnb1* function results in enhanced physiological response to provoked-epileptic seizures in zebrafish models reflecting an epileptiform-like electrographic activity.

2.7. No global morphological alterations neither brain anatomical defects in the kcnb1 mutant zebrafish model

In a review from Bar and collaborators (2020a) compiling data from the largest cohort of patients with *KCNB1*-DEEs, results revealed that 22% of patients exhibited abnormalities on brain magnetic resonance imaging (MRI). Specifically, findings included mild atrophy in 13%

(7/54), white matter abnormalities in 4% (2/54), focal cortical dysplasia in 2% (1/54), and bilateral periventricular heterotopia in 2% (1/54) (Bar et al., 2020a). The main morphological aspects and brain anatomical features of WT, *kcnb1*$^{+/-}$ and *kcnb1*$^{-/-}$ zebrafish lines were assessed at 48 hpf, 4 dpf and 6 dpf. Visual inspection of both *kcnb1* mutants (*kcnb1*$^{+/-}$ and *kcnb1*$^{-/-}$) did not reveal major morphological malformations at 48 hpf and 6 dpf compared to WT condition **(Figure 7A)**. Indeed, measurements of body length and head surface were similar between the different conditions at these two stages of development (body length at 6 dpf: *kcnb1*$^{+/+}$ = 3.45 ± 0.03 mm; *kcnb1*$^{+/-}$ = 3.82 ± 0.02 mm; *kcnb1*$^{-/-}$ = 3.62 ± 0.04 mm; +/+ *vs* mutants: p>0.5) **(Figure 7B)**. Further morphological parameters were analyzed such as the body surface, head length, eye diameter and surface, eye spacing, swim bladder and protruding mouth length at the same developmental stages **(Figure 7-figure supplement 4)**. The data do not show any major morphological differences between all conditions, with absence of body and head malformations (+/+ *vs* mutants: p>0.5) **(Figure 7-figure supplement 4)** confirmed by analyzing the global morphology of brain regions with the pan-neuronal marker HuC at 48 hpf and 4 dpf **(Figure 7C)**. Furthermore, we performed immunofluorescence on whole embryo and larvae at these same developmental time points (48 hpf and 6 dpf) and visualized in lateral and dorsal positions in order to visualize the Mautner cells **(**3A10 marker, **Figure 7D**) and neuronal fibers (acetylated tubulin, **Figure 7E**). Images were qualitatively analyzed, and the results did not reveal major neuronal loss or defects of organization due to *kcnb1* loss-of-function at the early stages of development **(Figure 7D, E),** as further confirmed by the quantification of Mauthner cell body length at 48 hpf (*kcnb1*$^{+/+}$ = 39.58 ± 2.26 µm; *kcnb1*$^{+/-}$ = 37.52 ± 0.86 µm; *kcnb1*$^{-/-}$ = 43.55 ± 1.96 µm; +/+ *vs* mutants: p>0.5) **(Figure 7-figure supplement 5)**. These results demonstrate that the *kcnb1* loss-of-function zebrafish model present a normal brain development similar to *KCNB1*-DEE patients presenting a normal brain MRI in major cases (78%) (Bar et al., 2020a).

2.8. kcnb1 mutant models do not present any alteration of muscle and neuromuscular junction organization but defect of acetylcholinesterase expression

Due to locomotor impairments and to further refine the phenotypic features in the *kcnb1* knock-out model, we performed an immunolabeling analysis of the muscle organization at 48 hpf. Global visualization of muscle fiber organization was performed using a brightfield microscope and by using Phalloidin preventing actin depolymerization **(Figure 8A)**. These analyzes were followed by labelling the two different and specific fiber components of muscle distinguished by their physiological properties: F310 marker highlighting type I fibers (fast muscle fibers) contracted for powerful and spontaneous forces and F59 marker to identity type II fibers (slow muscle fibers) mainly focused on balance and postural control **(Figure 8A).** In all the conditions, the fast muscle fibers were well organized in straight parallel lines as well as the slow muscle fibers which presented similar pattern at any stages of development. None of these results indicated any muscle impairments in both mutant models (*kcnb1*$^{+/-}$ and *kcnb1*$^{-/-}$) **(Figure 8A)** that were confirmed by applying two different methods of quantification comprising: 1) the anisotropy of fibrillar structures reflecting the organization of fibers (0 for no order and 1 for perfectly ordered i.e. parallel fibrils) and 2) the plot profile illustrating the relative distance between fibers for each muscle fiber (anisotropy of fast muscles (F310): *kcnb1*$^{+/+}$ = 0.443 ± 0.02; *kcnb1*$^{+/-}$ = 0.387 ± 0.06; *kcnb1*$^{-/-}$ = 0.51 ± 0.02; +/+ *vs* mutants: $p>0.5$) **(Figure 8B, C)**. Following the investigation on the muscle structure, we examined the organization of the neuromuscular junction (NMJ) organization at 48 hpf. An immunolabelling analysis was performed by targeting spinal motor neurons fibers (Znp1 marker) and acetylcholine receptor (AChR) clusters by using Bungarotoxin **(Figure 8D)**. At 48 hpf, we did not observe any disrupted arborization or axonal deficits of the spinal motor neuron projections on both *kcnb1*$^{+/-}$ and *kcnb1*$^{-/-}$ conditions as compared to WT larvae. Indeed, motor neurons had axonal projections and formed synapses along the length of muscle fibers for which the ratio

motor neuron length/spinal cord thickness was identical between all conditions (*kcnb1*$^{+/+}$ = 2.38 ± 0.11; *kcnb1*$^{+/-}$ = 2.43 ± 0.06; *kcnb1*$^{-/-}$ = 2.55 ± 0.14; +/+ *vs* mutants: p>0.5) **(Figure 8E)** and AchR puncta were similarly colocalizing with motoneuron branching **(Figure 8D)**. Quantification of mRNA subunits of AchR revealed identical composition at 6 dpf, where during development the chrn γ subunits (cholinergic receptor nicotinic) are substituted by chrn ε subunits (+/+ *vs* mutants: p>0.5) **(Figure 8G)**. Nevertheless, both mutant conditions (*kcnb1*$^{+/-}$ and *kcnb1*$^{-/-}$) presented significant decrease of acetylcholinesterase (AchE) mRNA expression, an enzyme involved in acetylcholine recycling at the NMJ level (*kcnb1*$^{+/+}$ = 1 ± 0 AU; *kcnb1*$^{+/-}$ = 0.48 ± 0.15 AU; *kcnb1*$^{-/-}$ = 0.37 ± 0.09 AU; +/+ *vs* +/-: p<0.5; +/+ *vs* -/-: p<0.1) **(Figure 8F)**. These results suggest that *kcnb1* is not involved in muscle and NMJ organization in zebrafish but conducts to a neurotransmission recycling defect at the NMJ.

3. Discussion

Mutations in *KCNB1* have recently been associated to developmental and epileptic encephalopathy (*KCNB1*-DEE) characterized by poor cognitive outcome and high frequency of drug-resistant epilepsy (Bar et al., 2020a, 2020b, 2022). Mouse models involving *kcnb1* knock-out and knock-in have provided insights into the behavioral features associated with *KCNB1*-DEE. These models exhibit behavioral and cognitive impairments, including locomotor hyperactivity and reduced anxiety-like behavior, along with lower thresholds for chemoconvulsant-induced seizures (Bortolami et al., 2022; Hawkins et al., 2021; Kang et al., 2024; Speca et al., 2014). However, mouse models have limitations due to the late onset of symptoms compared to the early manifestation of the disease in humans (Bortolami et al., 2022; Hawkins et al., 2021; Kang et al., 2024; Speca et al., 2014) and to the difficulty of high-throughput drug screening. Moreover, the underlying molecular pathways of *KCNB1*-DEE remain unclear and additional animal models may support our understanding of the disease.

The zebrafish has become an attractive alternative model for neurodevelopmental disorders allowing the evaluation of early developmental defects (Gawel et al., 2020a; Griffin et al., 2016).

We identified the presence of the kcnb1 protein with known RNA expression from 19 hpf (Jedrychowska et al., 2021) in various regions of the CNS, such as the Diencephalon, Midbrain, Hindbrain (including the cerebellum and the spinal cord) of wild type fish. However, kcnb1 was not detected in the telencephalon supporting the previous report by Shen et al. (2016). We showed that the partial or complete loss of *kcnb1* (*kcnb1*$^{+/-}$ and *kcnb1*$^{-/-}$) in embryonic and larval zebrafish causes early behavioral impairment and increased susceptibility to chemically induced seizures, thus recapitulating some of the key phenotypic features of *KCNB1*-DEE. These *kcnb1* mutants had no significantly increased mortality nor have morphological and anatomical abnormalities, which is consistent with the human early phenotype of *KCNB1*-DEE (Bar et al., 2020a). However, Jedrychowska et al. (2021) indicated that 48% of *kcnb1* mutants fish died within the three first month suggesting that *kcnb1* could be critical at later developmental stages. Moreover, we showed that *kcnb1* mutants (*kcnb1*$^{+/-}$ and *kcnb1*$^{-/-}$) had reduced tail coiling activity from 25 hpf until the end of this first behavioral period. Tail coiling activity was first used in general toxicological screening, to assess the developmental neurotoxicity of chemical products (Kokel et al., 2010; Ogungbemi et al., 2021; Raftery et al., 2014; Vliet et al., 2019). Two studies described a modification of this premotor activity in zebrafish models of *depdc5*-related epilepsy reporting opposite effect on coiling frequency, with a hyperactivity in the *depdc5* knock-down model at 28 hpf (de Calbiac et al., 2018) and coiling hypoactivity at 20 hpf in *depdc5* knock-out model (Swaminathan et al., 2018). This early stereotyped behavior is supported by synchronized spinal locomotor circuits mediated by the innervation of the muscle by the primary motor neurons, which are first present at around

17 hpf (Saint-Amant and Drapeau, 1998). The early Kv2.1 brain expression suggest that they might be implicated in motoneurons electrical functional pathways. The early hypoactive phenotype of our *kcnb1* models could therefore be linked to abnormal electrical neuronal activity resulting from the disruption of the synaptic neuronal activity in these embryonic neurons. While the morphological characteristics of neurons within the central nervous system (CNS) and motoneurons at the neuromuscular junction (NMJ) appeared similar to those of controls, as well as the abundance of acetylcholine receptor (AchR) puncta and the composition of AchR subunits, a notable reduction in the RNA expression level of AchE was observed in both *kcnb1* mutant fish. This finding is the first evidence of a neurotransmission impairment in this *kcnb1* loss-of-function model. At later stages of larval development, previous reports on both drug-induced and genetic models of epilepsy have revealed a stereotyped circular, corkscrew-like trajectory swimming characteristic of epileptogenic-like activity (Gawel et al., 2020a). We found a similar circular pattern of swim trajectories in *kcnb1* mutant models at the TEER test at 48 hpf, associated with increased swimming activity in both genotypes (*kcnb1*$^{+/-}$ and *kcnb1*$^{-/-}$), but revealed a huge variability in swimming behavior in the same condition, that we could separate into two distinct groups (mild and severe phenotypes). These results might reflect the variable spectrum of behavioral and cognitive impairments observed in patients (Bar et al., 2020b). Furthermore, *kcnb1*$^{-/-}$ mutants exhibited increased response of locomotor activity to a light-dark stimulus as compared to *kcnb1*$^{+/-}$ and wild-type lines. It has been demonstrated that light-to-dark transition induces a rapid increase in locomotor activity of zebrafish larvae, which decreases to baseline after a few 5–10 minutes (Burgess and Granato, 2007a, 2007b). This hyperactivity upon light switches is consistent with the increased locomotor activity found in previous *kcnb1* rodent models (Hawkins et al., 2021; Speca et al., 2014) and have been reported in valyl-tRNA synthetase (*vars*) knock-out zebrafish model, another genetic developmental and epileptic encephalopathy (Siekierska et al., 2019b). Using a succession of

audio stimuli, both *kcnb1* mutant (*kcnb1*$^{+/-}$ and *kcnb1*$^{-/-}$) models presented a decreased locomotor activity correlating with the results obtained by Jedrychowska et al. (2021). The zebrafish photomotor and hearing responses are regulated by neuronal connectivity of the hindbrain and spinal cord and multiple neurotransmitter pathways which could be disrupted by an abnormal neuronal activity related to *kcnb1* loss-of-function (Kokel et al., 2010).

The seizure-like behavior in *kcnb1* mutants (*kcnb1*$^{+/-}$ and *kcnb1*$^{-/-}$) is further supported by their increased locomotor activity characterized by fast circles trajectories induced by PTZ 5mM compared to wild-type. Indeed, these results are concomitant with the stage II of the "seizure-like behavior score" described by Baraban et al. (2005). Provoked-seizures induced by PTZ treatment were confirmed by acute neuronal hyperactivation in the telencephalon of *kcnb1*$^{-/-}$ fish obtained with c-Fos immunostaining. Moreover, the quantification of brain-derived neurotrophic factor (bdnf) mRNA in zebrafish larvae, a neurotrophin crucial for brain development and synaptic plasticity, revealed a significant upregulation of its expression level within the *kcnb1* knock-out zebrafish line (*kcnb1*$^{-/-}$). This finding indicates deficits in neurogenesis within the developing brain of homozygous transgenic fish. Similar results were obtained by identifying *c-Fos* and *bdnf* as genes associated with seizures in zebrafish, with increased expression levels observed after exposure to PTZ 20mM (Orellana-Paucar et al., 2013), the most used epileptic seizure inducer at larvae, juvenile and adult stages (Chitolina et al., 2023). These results were reinforced by polyspike discharges in both *kcnb1*$^{+/-}$ and *kcnb1*$^{-/-}$ fish, associated with an increase of the spikes number in *kcnb1*$^{+/-}$ fish after PTZ 40mM exposure. The absence of spontaneous seizures could reflect the existence of functional compensatory pathways masking the phenotypic features due to reduced levels of *kcnb1*. Electrophysiological recordings unveiled also a variability within the same genotype, which delineated two distinct phenotypes: mild and severe. In addition, electrophysiological

recordings and immunostaining of c-Fos were 1) conducted in distinct brain regions, namely the optic tectum and the telencephalon and 2) done using different concentrations of PTZ, precluding a direct correlation between the findings. Therefore, these results are in favor of an essential role of *kcnb1* in electrical neuronal functions during the early development of zebrafish brain.

The list of confirmed genes associated with developmental and epileptic encephalopathies is expanding, yet the progress in developing targeted treatments is notably sluggish. Our investigation suggests that the zebrafish model of *kcnb1* loss-of-function provides a valuable model to reproduce some key features of *KCNB1*-DEE. These include early behavioral disturbances, increased susceptibility to seizures, and impaired neuronal function in the developing brain of embryo and larvae brain. Both *kcnb1*$^{+/-}$ and *kcnb1*$^{-/-}$ zebrafish models recapitulate these, underscoring the central role of *kcnb1* loss-of-function in the pathogenesis of these disorders. The larval zebrafish model is suitable for studying the neuropathogenesis of *KCNB1*-DEE and may facilitate high-throughput drug screening, opening the possibilities of repurposing or testing for new therapeutic compounds aiming the prognosis and quality of life of individuals with *KCNB1*-DEE.

5. Materials and methods

5.1. Housing conditions of zebrafish

Adult zebrafish lines (Danio Rerio) were housed in a conventional animal facility at the IMAGINE Institute (Institut des Maladies Génétiques, INSERM U1163, Paris, France) and bred according to the National and European Guidelines for Animal Welfare. Experiments were performed on wild-type AB and TU strains (Tübingen, Germany) and from the *kcnb1* mutant zebrafish lines (Shen et al., 2016) aged between 0- and 6-days post-fertilization. Fertilized eggs

were collected by natural spawning. Embryos and larvae were exposed to artificial lighting in a 14h/10h nycthemeral cycle (daytime: 8h-10h), maintained in an incubator at controlled temperature of 28 ± 1 °C and preserved in embryo medium: 0.33 mM $CaCl_2$; 0.33 mM $MgSO_4$; 5 mM NaCl; 0.17 mM KCl; pH7.4 (Instant Ocean, Blacksburg, Virginia, USA) complemented with 0.01 mg/L methylene blue. Embryos and larvae were staged in hours post-fertilization (hpf) and days post-fertilization (dpf) (Kimmel et al., 1995). All procedures involving zebrafish embryos, larvae and adults were approved by the Institutional Ethics Committees at the Research Centers of Imagine Institute and were performed in accordance with the European Union Directive (2010/63/EU).

5.2. kcnb1 mutant zebrafish lines

Heterozygous embryos from *kcnb1* mutant zebrafish line (*kcnb1*$^{+/-}$) were kindly provided by the team of Dr. Vladimir Korzh (International Institute of Molecular and Cell Biology of Warsaw, Poland). This *kcnb1* mutant line was generated by CRISPR/Cas9 mutagenesis targeting the GGAGCTGGACTACTGGGGAG sequence in the first exon of the gene and permitting a 2-G bases deletion and an insertion of a 14 bp-nucleotide sequence: ATCTCATCCACTAA (2 bp deleted/14 bp inserted: CC/TTAGTGGATGAGAT), resulting in a premature stop codon between the N-terminal cytoplasmic domain and the first transmembrane domain (Shen et al., 2016). We raised *kcnb1*$^{+/-}$ mutant fish until adulthood and we then crossed *kcnb1*$^{+/–}$ males and *kcnb1*$^{+/–}$ females to obtain *kcnb1*$^{-/-}$ zebrafish mutant lines for all experiments. *Kcnb1*$^{-/-}$ mutant fish (also referred as *kcnb1*$^{sq301/sq301}$, reference ID zfin: ZDB-ALT-170417-2, indel mutation) were first described by Shen et al. (2016).

5.3. Genotyping of kcnb1 mutant lines

Genomic DNA of adult fish was extracted by boiling the caudal fin in extraction DNA solution (25 mM NaOH / 0.2 mM EDTA) followed by Tris-HCl neutralization buffer (40 mM, pH 5.4). Samples were amplified by PCR using DreamTaq Hot Start PCR Master Mix (Thermo

Scientific, Waltham, Massachusetts, USA, #K9012) with the following primers targeting *kcnb1* (10 mM): F_5'-TGTGACGACTACAACCTGGA-3' and R_5'-CTCCTCGTTCATCTGCTCCT-3'. The PCR was performed in a T100 Thermal Cycler (Bio-Rad, Hercules, California, USA) and DNA samples were sent for sequencing to GATC Biotech, Eurofins Genomics (Nantes, France).

Genotyping was in parallel performed by high resolution melting analysis (HRMA). Samples were amplified with BlasTaq 2X qPCR Master Mix (abm, Canada, #G892) and the CFX384 Touch Real-Time PCR Detection System (Bio-Rad, USA) Curves were analyzed using the Bio-rad CFX Maestro software V4.1.2433.1219 (Bio-Rad, USA). The curve shifts correctly identified the presence of the mutated allele.

5.4. Survival assay

Embryos and larvae were checked daily and maintained in Petri dish in a 28 ± 1 °C incubator from 0 dpf to 6 dpf. After 6 dpf, larvae were transferred in tanks with dripped water flux. Survival was assessed from 0 to 15 dpf and fish were fed regularly. Survival refers to the number of living individuals relative to the total number at a given time.

5.5. RT-qPCR

6 dpf-larvae zebrafish were anesthetized in ice (30 fish individuals/pool). Total RNA was extracted using TRIzol reagent (Euromedex, Souffelweyersheim, France, #TR118) and Chloroform (Sigma-Aldrich, Saint-Louis, Missouri, USA, #366927) according to the manufacturer's protocol followed by the purification of RNA using the GeneJET RNA Cleanup and Concentration micro-Kit (Thermo Scientific, USA, #K0841) including DNA removal step and using DNase I (Thermo Scientific, USA, #EN0521). RNA concentration was quantified using the Nanodrop 2000 Spectrophotometer (Thermo Scientific, USA) and samples were synthesized using a 5X All-In-One RT MasterMix (abm, Canada, #G592) before using the T100 Thermal Cycler (Bio-Rad, USA).

For qPCR, gene specific primers were used in an amplification reaction with BlasTaq 2X qPCR Master Mix (abm, Canada, #G892) on a BioRad CFX384 Real Time PCR System (Bio-Rad, USA). Data were analyzed with CFX Manager software (Bio-Rad, USA). The relative expression of gene levels was determined using the comparative $2^{-\Delta\Delta Ct}$ method (Livak and Schmittgen, 2001). The amount of gene cDNA was normalized from housekeeping genes *β-actin* or *ef1α* (see primers used in **Table 1**). Results were obtained from three to four independent crosses with samples analyzed in triplicate and the condition *kcnb1*$^{+/+}$ is considered as the reference value (relative fold change = 1).

5.6. Morphological analysis

WT, *kcnb1*$^{+/-}$ and *kcnb1*$^{-/-}$ at 48 hpf and 6 dpf were screened for morphological abnormalities. They were maintained in a Petri dish containing embryo medium complemented with 3% Methylcellulose (Sigma-Aldrich, USA, #274429) to allow dorsal and lateral pictures of the whole body on glass microscope slides. Images were acquired with a stereomicroscope (SZX16, Olympus Life Science, Hamburg, Germany) equipped with a Blackfly S BFS-U3-04S2M-CS camera (FLIR Systems Inc., Wilsonville, Oregon, USA) and SpinView V2.0.0.147 software (FLIR Systems Inc., USA). Measurements were performed manually with ImageJ software (National Institutes of Health, NIH, New-York, USA). Body, head, swim bladder, eye and protruding mouth parameters–were measured by following areas of interest using some predetermined spots.

5.7. Locomotion assessment

Premotor activity. Spontaneous tail coiling activity in zebrafish embryos was recorded every hour from 24 hpf to 36 hpf. Groups of 10 embryos inside their chorion were arrayed into a 100 mm Petri dish filled with embryo medium and placed on a plastic mesh (1.2 x 1.2 mm). An acclimation period of 5 min was defined to avoid coiling due to embryos transfer and manipulation. Sixty-second movies were obtained under a stereomicroscope with darkfield

illumination (SZX16, Olympus Life Science, Germany) with a Blackfly S BFS-U3-04S2M-CS camera (FLIR Systems lnc., USA), recorded at a frame rate of 30 frames per second (fps) using SpinView V2.0.0.147 software (FLIR Systems lnc., USA). Movies were obtained in Motion-JPEG compression format and visualized on ImageJ software (NIH). Embryos coiling or tail flicking events for the controls and *kcnb1* deletion mutants were counted manually.

Touch-evoked escape response (TEER). 48 hpf-zebrafish embryos were manually dechorionated and morphologically normal fish were placed in the center of a 15-cm diameter petri dish filled with embryo water at room temperature (RT). A mechanical stimulus was applied at the level of the tail of embryos using a plastic pipette tip to trigger the TEER. The trajectory of individual embryos was recorded with a Blackfly S BFS-U3-04S2M-CS camera (FLIR Systems lnc., USA) at 30 fps using SpinView V2.0.0.147 software (FLIR Systems lnc., USA). The swimming trajectory was traced using the Manual Tracking Plug-in (https://imagej.nih.gov/ij/plugins/manual-tracking.html) in ImageJ software (NIH). A macro script on Excel (Microsoft, Redmond, USA) designed by the team allowed to obtain the x–y coordinates which were used to calculate the distance (in mm), velocity (mm/s), time spent in motion (s) and to have a view of the global trajectory of each embryo.

Spontaneous locomotion. A ViewPoint V.5.25.0.0 (Viewpoint Life Sciences, Montpellier, France) setup combined with an automated computer recording system equipped with Zebralab 438 software (Viewpoint Life Sciences, France) was used to measure spontaneous locomotor activity of zebrafish larvae. Larvae were placed in a 48-well plate (one larva per well, Fisher Scientific, USA) filled with 500 μL of embryo medium. Fish were acclimatized to wells in a Zebrabox (Viewpoint Life Sciences, France) with lights off for 15 min at 28.5°C prior to recording. Larvae were submitted to two different protocols: 1) a light-induced protocol of 60 minutes recording split into 10 min blocks alternating light and dark conditions repeated three times (the locomotor activity was analyzed during the whole protocol)

and 2) a sound-induced protocol of four repeated audio stimuli (450 hertz, 80 decibel) during one second separated by 10 min of silence (the locomotor activity was analyzed five seconds after each stimulus). Video recordings were performed at the same time during the day. Locomotion plots were obtained for one fish per well and were analyzed for total distance travelled (in centimeters). Experiments were done each day from 3 to 6 dpf on the same fish. All tracking experiments were performed in at least triplicate.

Behavioral analysis of pentylenetetrazol (PTZ)-induced seizures. 3 to 6 dpf-zebrafish larvae were placed in a 48-well plate (one larva per well, Fisher Scientific, USA) filled with embryo medium. After acclimation in the Zebrabox (Viewpoint Life Sciences, France) in the dark, larval activity was recorded using the tracking feature of the ViewPoint V.5.25.0.0 software (Viewpoint Life Sciences, France) for 30 min to determine baseline activity levels for each fish. After the baseline activity run, fresh PTZ (stock solution of 200 mM, Sigma-Aldrich, USA, # P6500) was added to each well for a final concentration of 5 mM PTZ. Larvae activity was then recorded for a further 30 min to determine larval responses to PTZ. Each experimental assay was performed at the same relative time of day and repeated at least three times and the locomotor activity was analyzed during the whole protocol.

5.8. Electrophysiological analysis

Zebrafish larvae at 5 and 6 dpf were embedded in 1% low-melting temperature agarose diluted into MilliQ water (Sigma-Aldrich, USA). The fish were covered with artificial cerebro-spinal fluid (ACSF) containing (in mM): HEPES 10, NaCl 134, KCl 2.9, $CaCl_2$ 2.1, $MgCl_2$ 1.2, glucose 10 (pH 7.8, osmolarity to 290-295 mOsm/l). The dorsal side of larvae was visible to allow correct implantation of the electrode in the brain. A borosilicate glass electrode with a resistance of 2–7 MΩ and a tip diameter of approximately 1 μm was filled with ACSF and implanted into the optic tectum, using an Olympus microscope (Infinity 3S, 10X magnification, Olympus Life Science, Germany). Local field potential (LFP) recordings were obtained in

current-clamp mode using a MultiClamp700B amplifier (Molecular devices, San José, California, USA) and an Axon Digidata 1550 (Molecular devices, USA). All recordings were acquired using a low-pass filter of 1 Hz, a high-pass filter of 1 kHz, and a digital gain of 10. We compared neuronal activity between controls and *kcnb1* mutant zebrafish larvae from baseline recordings of 30 min duration. To chemically induce epileptiform-like electrographic activity, PTZ (stock solution of 200 mM, Sigma-Aldrich, USA, # P6500) dissolved in ACSF was added to the recording chamber at a final concentration of 40 mM and the recording continued for 30 min. Neuronal activity was recorded using Clampex V11.1 software (Molecular devices, USA) coupled with MultiClamp 700B commander (Molecular devices, USA). Fish were frequently observed under microscope to confirm that they were alive during the recording by assessing blood flow and heartbeat. The number of negative spikes was automatically analyzed using Clampfit V11.2 software during a 10 min interval in the middle of each analysis period (Molecular devices, USA) (see **Figure 8A**).

5.9. Immunohistochemistry on slices

Zebrafish aged from 48 hpf to 6 dpf were fixed in 4% formaldehyde, 1X Phosphate Buffered Saline (1X PBS) for 30 minutes at RT and stored at -80°C in an individual frozen block of Gelatin 15%, Sucrose 7,5% until use. After obtaining horizontal or transversal brain slices of embryos and larvae using the cryostat CM3050 S (Leica, Wetzlar, Germany), the slices were rinsed several times with 1X PBS and then incubated for 30 minutes in blocking solution containing 1X PBS, 0,1% Triton-20X, 2% Gelatin and 3% BSA. The embryos were incubated overnight at 4°C in 1:100 dilution of rabbit anti-HuC antibody (Tebubio, Le Perray-en-Yvelines, France, #FNab04072) or goat anti-Kcnb1 antibody (Tebubio, France, #PAB7569) diluted in blocking solution. The embryos were then washed several times with blocking solution and incubated for 1h in blocking solution containing a secondary antibody Alexa Fluor 647 (Thermo Scientific, USA, #A-21244, 1:250) or Alexa Fluor 488 (Thermo Scientific, USA,

#A11055, 1:250) for 2h at RT. Brain slices were then incubated during 10 minutes at RT of DAPI (Invitrogen, Waltham, Massachusetts, USA, #D3571, 1:1000) followed by mounting on glass slide in Immu-Mount mounting medium (Epredia, Neuilly-sur-Seine, France, #9990402). The brains were visualized using a Spinning disk system (Carl Zeiss, Oberkochen, Germany). Images were captured between magnification 10x and 63x.

5.10. Whole-mount immunohistochemistry

Whole-mount immunohistochemistry on 48 hpf-embryos and 6 dpf-larvae was performed according to a previously established protocol (Santos et al., 2018). Embryos were treated with 0,003% 1-Phenyl-2-thiourea (PTU) (Sigma-Aldrich, USA, #P7629) to prevent pigmentation of the skin and to avoid any interference on the regions of interest during acquisition. Briefly, fish were fixed with 4% formaldehyde (Sigma-Aldrich, USA, #158127) diluted in 1X PBS for 2h at RT. Fish were then dehydrated with in increased percentages of methanol (25%, 50% and 75%) before being stored at -20°C in 100% methanol. After a gradual rehydration in 75%, 50% and 25% methanol and several washes in 1X PBS, the embryos/larvae were permeabilized in fresh acetone for 20 min. Fish were blocked and permeabilized with 10% Bovine standard-albumin (BSA) (Eurobio Scientific, Les Ulis, France, #HALALB07-65) in 1X PBS – 0,1% Tween-20X solution (PBST 0,1%) overnight at 4°C. Fish were incubated with the primary antibody diluted 1% BSA / 0,1% PBST at 4°C for at least two days. After washing in 0,1% PBST, fish were incubated with the secondary antibody in 1% BSA / 0,1% PBST overnight at 4°C. After washes and passing through increased percentages of glycerol 25%, 50% and 75% (Sigma-Aldrich, USA, #G9012), embryos and larvae were maintained in 100% glycerol until image acquisition under a confocal microscopy (Spinning Disk, Carl Zeiss, Germany). Images were taken using 100% glycerol to allow lateral and dorsal positioning of the fish. The same brightness and contrast values were applied to all images using Zen blue edition V2.6 (Carl Zeiss Microscopy GmbH, 2018).

Primary antibodies used were mouse anti-acetylated tubulin antibody (1:100, Sigma-Aldrich, USA, #T7451), mouse anti-3A10 antibody (1:100, DSHB, Iowa City, Iowa, USA, #3A10), mouse anti-F310 antibody (1:100, DSHB, USA, #F310), mouse anti-F59 antibody (1:20, DSHB, USA, #F59), mouse anti-Znp1 antibody (1:100, DSHB, USA, #znp1) and mouse anti-c-Fos antibody (1:100, Santa Cruz Biotechnology, Dallas, Texas, USA, #sc-166940). Secondary antibodies used were goat anti-mouse Alexa Fluor 488 (Thermo Scientific, USA, #A11001), goat anti-mouse Alexa Fluor 647 (Thermo Scientific, USA, #A21235), goat anti-rat Alexa Fluor 647 (Thermo Scientific, USA, #A21247) and goat anti-rabbit Alexa Fluor 647 (Thermo Scientific, USA, #A-21244), all used at a dilution of 1:250. CoraLite® Plus 488-Phalloidin (1:50, ProteinTech, Chicago, USA, #PF00001) and α-Bungarotoxin Alexa 594 (1:10, Abcam, Cambridge, UK, #ab120542) respectively preventing actin depolymerization F-actin and blocking acetylcholine receptors (AchR) activation , were used following the protocol described by Goody and Henry (2013).

Based on whole-mount immunohistochemistry of fish, muscle organization was analyzed using two different methods: 1) the quantification of the anisotropy of fibrillar structures in raw images of Phalloidin, F310 and F59 labelling using the plugin FibrilTool from the software ImageJ (Boudaoud et al., 2014). A Gaussian filter was applied on images and the anisotropy was analyzed reflecting the organization of fibers following the convention: 0 for no order and 1 for perfectly ordered (parallel fibrils) and 2) by obtaining a plot profile illustrating the relative distance between fibers for each muscle fibers labelling (Phalloidin, F310 and F59).

Concerning the c-Fos labelling, the number of c-Fos positive-neurons and the fluorescence intensity value of c-Fos per neuron were quantified using the software IMARIS (Oxford Instruments, version 10.1.0, Abingdon-on-Thames, United Kingdom) and by analyzing the telencephalon, the major region activated after the chemical treatment. The contour of the region of interest has been designed manually to obtain the volume (μm^3) of the telencephalon,

neurons were then identified automatically within the region following identical parameters for spot detection between conditions and visualized in 3 dimensions to avoid false negative spots. Values were normalized according to the volume of the telencephalon. Furthermore, the distribution (in %) of c-Fos positive-neurons according to the fluorescence intensity value of c-Fos in the telencephalon of fish at 6 dpf, reflecting the level of neuronal activation, that was divided in four equal shares (from 0 to 100%): low (0-25%), moderately low (25-50%), moderately high (50-75%) and high (75-100%) neuronal activation.

5.11. Statistical analysis

For all experiments, *kcnb1* knock-out models (*kcnb1*$^{+/-}$ and *kcnb1*$^{-/-}$) were compared to WT (*kcnb1*$^{+/+}$). Figures comprising immunohistochemistry images have been made using a Fiji plugin: FigureJ. Statistical analysis was performed using GraphPad Prism 8 version software (GraphPad Software, San Diego, California, USA). Normality was determined by the Shapiro-Wilk test. Multiple comparisons were performed using one or two-way ANOVA (Analysis of Variance) tests followed by Tukey's post-hoc test or Kruskal-Wallis test followed by Dunn's post-hoc. Experiments presenting less than 10 values per conditions were analyzed using the non-parametric Mann-Whitney test. Statistical tests used are specified in the legend of each figure. Values represent the mean ± standard error of the mean (SEM). Results were considered significant if the p-value was < 0.05. For all experiments, at least 3 single experiments were performed (N) with a certain number of embryos or larvae per condition (n).

Authors contributions

L.R. and C.B. designed experiments. L.R performed zebrafish experimentation, imaging and analyzed the data. L.L performed part of locomotor activity experiments on fish. L.R. and S.C. were responsible for the electrophysiological recordings. L.R. performed electrophysiological analysis. A.M and S.R were responsible of technical support. E.K., S.C. and R.N. were

responsible for the project coordination. L.R. and C.B. were responsible for the writing of this report. E.K., S.C. and R.N. revised the paper accordingly and approved the manuscript. All authors revised the final version of the manuscript.

Acknowledgements

We are grateful of the team of Dr. Vladimir Korzh (International Institute of Molecular and Cell Biology of Warsaw, Poland) for kindling provided us the *kcnb1* knock-out transgenic zebrafish line. We appreciate the help of the LEAT Zebrafish facilities and Cell Imaging Facility of Imagine Institute for respectively fish maintenance and expert technical help. The help of Nicolas Goudin, responsible of the Image analysis center of SFR Necker (Paris, France) was highly appreciated for immunofluorescence quantification. We thank DSHB for the antibodies used for whole-mount immunohistochemistry: 3A10 was deposited to the DSHB by Jessell, T.M. / Dodd, J. / Brenner-Morton, S. (DSHB Hybridoma Product 3A10), F310 was deposited to the DSHB by Stockdale, F.E. (DSHB Hybridoma Product F310), F59 was deposited to the DSHB by Stockdale, F.E. (DSHB Hybridoma Product F59), Znp-1 was deposited to the DSHB by Trevarrow, B. (DSHB Hybridoma Product znp-1), mAb 35 was deposited to the DSHB by Lindstrom, J. (DSHB Hybridoma Product mAb 35).

Funding

This work was supported by grants from the Agence Nationale de la Recherche under “Investissements d’avenir” program (ANR-10IAHU-01), the Fondation Bettencourt Schueller (C.B. and R.N.), the Ligue Française Contre l'Épilepsie (C.B), the ERC Consolidator Grant (E.K.). R.N and L.R are supported by the Chair Geen-DS funded by FAMA fund hosted by Swiss Philanthropy Foundation. L.R is recipient of a grant from the Fondation pour la Recherche Médicale (grant number: PLP202009012460, 2021).

Declaration of interest: The authors declare that no conflict of interest exists.

References

Afrikanova, T., Serruys, A.-S.K., Buenafe, O.E.M., Clinckers, R., Smolders, I., de Witte, P.A.M., Crawford, A.D., Esguerra, C.V., 2013. Validation of the Zebrafish Pentylenetetrazol Seizure Model: Locomotor versus Electrographic Responses to Antiepileptic Drugs. PLoS ONE 8, e54166. https://doi.org/10.1371/journal.pone.0054166

Antonucci, D.E., Lim, S.T., Vassanelli, S., Trimmer, J.S., 2001. Dynamic localization and clustering of dendritic Kv2.1 voltage-dependent potassium channels in developing hippocampal neurons. Neuroscience 108, 69–81. https://doi.org/10.1016/S0306-4522(01)00476-6

Bar, C., Barcia, G., Jennesson, M., Le Guyader, G., Schneider, A., Mignot, C., Lesca, G., Breuillard, D., Montomoli, M., Keren, B., Doummar, D., Billette de Villemeur, T., Afenjar, A., Marey, I., Gerard, M., Isnard, H., Poisson, A., Dupont, S., Berquin, P., Meyer, P., Genevieve, D., De Saint Martin, A., El Chehadeh, S., Chelly, J., Guët, A., Scalais, E., Dorison, N., Myers, C.T., Mefford, H.C., Howell, K.B., Marini, C., Freeman, J.L., Nica, A., Terrone, G., Sekhara, T., Lebre, A., Odent, S., Sadleir, L.G., Munnich, A., Guerrini, R., Scheffer, I.E., Kabashi, E., Nabbout, R., 2020a. Expanding the genetic and phenotypic relevance of *KCNB1* variants in developmental and epileptic encephalopathies: 27 new patients and overview of the literature. Hum. Mutat. 41, 69–80. https://doi.org/10.1002/humu.23915

Bar, C., Kuchenbuch, M., Barcia, G., Schneider, A., Jennesson, M., Le Guyader, G., Lesca, G., Mignot, C., Montomoli, M., Parrini, E., Isnard, H., Rolland, A., Keren, B., Afenjar, A.,

Dorison, N., Sadleir, L.G., Breuillard, D., Levy, R., Rio, M., Dupont, S., Negrin, S., Danieli, A., Scalais, E., De Saint Martin, A., El Chehadeh, S., Chelly, J., Poisson, A., Lebre, A.S., Nica, A., Odent, S., Sekhara, T., Brankovic, V., Goldenberg, A., Vrielynck, P., Lederer, D., Maurey, H., Terrone, G., Besmond, C., Hubert, L., Berquin, P., Billette de Villemeur, T., Isidor, B., Freeman, J.L, Mefford, H.C., Myers, C.T., Howell, K.B., Rodríguez-Sacristán Cascajo, A., Meyer, P., Genevieve, D., Guët, A., Doummar, D., Durigneux, J., van Dooren, M.F., de Wit, M.C.Y., Gerard, M., Marey, I., Munnich, A., Guerrini, R., Scheffer, I.E., Kabashi, E., Nabbout, R., 2020b. Developmental and epilepsy spectrum of *KCNB1* encephalopathy with long-term outcome. Epilepsia. 61(11), 2461–2473. https://doi-org/10.1111/epi.16679

Bar, C., Breuillard, D., Kuchenbuch, M., Jennesson, M., Le Guyader, G., Isnard, H., Rolland, A., Doummar, D., Fluss, J., Afenjar, A., Berquin, P., De Saint Martin, A., Dupont, S., Goldenberg, A., Lederer, D., Lesca, G., Maurey, H., Meyer, P., Mignot, C., Nica, A., Odent, S., Poisson, A., Scalais, E., Sekhara, T., Vrielynck, P., Barcia, G., Nabbout, R., 2022. Adaptive behavior and psychiatric comorbidities in KCNB1 encephalopathy. Epilepsy Behav. 126, 108471. https://doi.org/10.1016/j.yebeh.2021.108471

Baraban, S.C., Dinday, M.T., Hortopan, G.A., 2013. Drug screening in Scn1a zebrafish mutant identifies clemizole as a potential Dravet syndrome treatment. Nat. Commun. 4, 2410. https://doi.org/10.1038/ncomms3410

Baraban, S.C., Taylor, M.R., Castro, P.A., Baier, H., 2005. Pentylenetetrazole induced changes in zebrafish behavior, neural activity and c-fos expression. Neuroscience 131, 759–768. https://doi.org/10.1016/j.neuroscience.2004.11.031

Bishop, H.I., Guan, D., Bocksteins, E., Parajuli, L.K., Murray, K.D., Cobb, M.M., Misonou, H., Zito, K., Foehring, R.C., Trimmer, J.S., 2015. Distinct Cell- and Layer-Specific Expression Patterns and Independent Regulation of Kv2 Channel Subtypes in Cortical

Pyramidal Neurons. J. Neurosci. 35, 14922–14942. https://doi.org/10.1523/JNEUROSCI.1897-15.2015

Bortolami, A., Yu, W., Forzisi, E., Ercan, K., Kadakia, R., Murugan, M., Fedele, D., Estevez, I., Boison, D., Rasin, M.-R., Sesti, F., 2022. Integrin-KCNB1 potassium channel complexes regulate neocortical neuronal development and are implicated in epilepsy. Cell Death Differ. https://doi.org/10.1038/s41418-022-01072-2

Boudaoud, A., Burian, A., Borowska-Wykręt, D., Uyttewaal, M., Wrzalik, R., Kwiatkowska, D., Hamant, O., 2014. FibrilTool, an ImageJ plug-in to quantify fibrillar structures in raw microscopy images. Nat. Protoc. 9, 457–463. https://doi.org/10.1038/nprot.2014.024

Burgess, H.A., Granato, M., 2007a. Modulation of locomotor activity in larval zebrafish during light adaptation. J. Exp. Biol. 210, 2526–2539. https://doi.org/10.1242/jeb.003939

Burgess, H.A., Granato, M., 2007b. Sensorimotor Gating in Larval Zebrafish. J. Neurosci. 27, 4984–4994. https://doi.org/10.1523/JNEUROSCI.0615-07.2007

Chitolina, R., Gallas-Lopes, M., Reis, C.G., Benvenutti, R., Stahlhofer-Buss, T., Calcagnotto, M.E., Herrmann, A.P., Piato, A., 2023. Chemically-induced epileptic seizures in zebrafish: A systematic review. Epilepsy Res. 197, 107236. https://doi.org/10.1016/j.eplepsyres.2023.107236

Crouzier, L., Richard, E.M., Sourbron, J., Lagae, L., Maurice, T., Delprat, B., 2021. Use of Zebrafish Models to Boost Research in Rare Genetic Diseases. Int. J. Mol. Sci. 22, 13356. https://doi.org/10.3390/ijms222413356

de Calbiac, H., Dabacan, A., Marsan, E., Tostivint, H., Devienne, G., Ishida, S., Leguern, E., Baulac, S., Muresan, R.C., Kabashi, E., Ciura, S., 2018. Depdc5 knockdown causes mTOR-dependent motor hyperactivity in zebrafish. Ann. Clin. Transl. Neurol. 5, 510–523. https://doi.org/10.1002/acn3.542

de Kovel, C.G.F., Syrbe, S., Brilstra, E.H., Verbeek, N., Kerr, B., Dubbs, H., Bayat, A., Desai, S., Naidu, S., Srivastava, S., Cagaylan, H., Yis, U., Saunders, C., Rook, M., Plugge, S., Muhle, H., Afawi, Z., Klein, K.-M., Jayaraman, V., Rajagopalan, R., Goldberg, E., Marsh, E., Kessler, S., Bergqvist, C., Conlin, L.K., Krok, B.L., Thiffault, I., Pendziwiat, M., Helbig, I., Polster, T., Borggraefe, I., Lemke, J.R., van den Boogaardt, M.-J., Møller, R.S., Koeleman, B.P.C., 2017. Neurodevelopmental Disorders Caused by De Novo Variants in *KCNB1* Genotypes and Phenotypes. JAMA Neurol. 74, 1228. https://doi.org/10.1001/jamaneurol.2017.1714

Du, J., Tao-Cheng, J.-H., Zerfas, P., McBain, C.J., 1998. The K+ channel, Kv2.1, is apposed to astrocytic processes and is associated with inhibitory postsynaptic membranes in hippocampal and cortical principal neurons and inhibitory interneurons. Neuroscience 84, 37–48. https://doi.org/10.1016/S0306-4522(97)00519-8

Gawel, K., Langlois, M., Martins, T., van der Ent, W., Tiraboschi, E., Jacmin, M., Crawford, A.D., Esguerra, C.V., 2020a. Seizing the moment: Zebrafish epilepsy models. Neurosci. Biobehav. Rev. 116, 1–20. https://doi.org/10.1016/j.neubiorev.2020.06.010

Gawel, K., Turski, W.A., van der Ent, W., Mathai, B.J., Kirstein-Smardzewska, K.J., Simonsen, A., Esguerra, C.V., 2020b. Phenotypic Characterization of Larval Zebrafish (Danio rerio) with Partial Knockdown of the cacna1a Gene. Mol. Neurobiol. 57, 1904–1916. https://doi.org/10.1007/s12035-019-01860-x

Goody, M., Henry, C., 2013. Phalloidin Staining and Immunohistochemistry of Zebrafish Embryos. BIO-Protoc. 3. https://doi.org/10.21769/BioProtoc.786

Griffin, A., Krasniak, C., Baraban, S.C., 2016. Advancing epilepsy treatment through personalized genetic zebrafish models, in: Progress in Brain Research. Elsevier, pp. 195–207. https://doi.org/10.1016/bs.pbr.2016.03.012

Grone, B.P., Marchese, M., Hamling, K.R., Kumar, M.G., Krasniak, C.S., Sicca, F., Santorelli, F.M., Patel, M., Baraban, S.C., 2016. Epilepsy, Behavioral Abnormalities, and Physiological Comorbidities in Syntaxin-Binding Protein 1 (STXBP1) Mutant Zebrafish. PLOS ONE 11, e0151148. https://doi.org/10.1371/journal.pone.0151148

Hawkins, N.A., Misra, S.N., Jurado, M., Kang, S.K., Vierra, N.C., Nguyen, K., Wren, L., George, A.L., Trimmer, J.S., Kearney, J.A., 2021. Epilepsy and neurobehavioral abnormalities in mice with a dominant-negative KCNB1 pathogenic variant. Neurobiol. Dis. 147, 105141. https://doi.org/10.1016/j.nbd.2020.105141

Hermann, A., Sitdikova, G., Weiger, T., 2015. Oxidative Stress and Maxi Calcium-Activated Potassium (BK) Channels. Biomolecules 5, 1870–1911. https://doi.org/10.3390/biom5031870

Ibhazehiebo, K., Rho, J.M., Kurrasch, D.M., 2020. Metabolism-based drug discovery in zebrafish: An emerging strategy to uncover new anti-seizure therapies. Neuropharmacology 167, 107988. https://doi.org/10.1016/j.neuropharm.2020.107988

Jedrychowska, J., Gasanov, E.V., Korzh, V., 2021. Kcnb1 plays a role in development of the inner ear. Dev. Biol. 471, 65–75. https://doi.org/10.1016/j.ydbio.2020.12.007

Johnson, B., Leek, A.N., Solé, L., Maverick, E.E., Levine, T.P., Tamkun, M.M., 2018. Kv2 potassium channels form endoplasmic reticulum/plasma membrane junctions via interaction with VAPA and VAPB. Proc. Natl. Acad. Sci. 115. https://doi.org/10.1073/pnas.1805757115

Kang, S.K., Hawkins, N.A., Thompson, C.H., Baker, E.M., Echevarria-Cooper, D.M., Barse, L., Thenstedt, T., Dixon, C.J., Speakes, N., George, A.L., Kearney, J.A., 2024. Altered neurological and neurobehavioral phenotypes in a mouse model of the recurrent KCNB1-p.R306C voltage-sensor variant. Neurobiol. Dis. 194, 106470. https://doi.org/10.1016/j.nbd.2024.106470

Kang, S.K., Vanoye, C.G., Misra, S.N., Echevarria, D.M., Calhoun, J.D., O'Connor, J.B., Fabre, K.L., McKnight, D., Demmer, L., Goldenberg, P., Grote, L.E., Thiffault, I., Saunders, C., Strauss, K.A., Torkamani, A., der Smagt, J., Gassen, K., Carson, R.P., Diaz, J., Leon, E., Jacher, J.E., Hannibal, M.C., Litwin, J., Friedman, N.R., Schreiber, A., Lynch, B., Poduri, A., Marsh, E.D., Goldberg, E.M., Millichap, J.J., George, A.L., Kearney, J.A., 2019. Spectrum of Kv2.1 Dysfunction in KCNB1-Associated Neurodevelopmental Disorders. Ann. Neurol. 86, 899–912. https://doi.org/10.1002/ana.25607

Kimmel, C.B., Ballard, W.W., Kimmel, S.R., Ullmann, B., Schilling, T.F., 1995. Stages of embryonic development of the zebrafish. Dev. Dyn. 203, 253–310. https://doi.org/10.1002/aja.1002030302

Kokel, D., Bryan, J., Laggner, C., White, R., Cheung, C.Y.J., Mateus, R., Healey, D., Kim, S., Werdich, A.A., Haggarty, S.J., MacRae, C.A., Shoichet, B., Peterson, R.T., 2010. Rapid behavior-based identification of neuroactive small molecules in the zebrafish. Nat. Chem. Biol. 6, 231–237. https://doi.org/10.1038/nchembio.307

Kolesnikova, T.O., Demin, K.A., Costa, F.V., Zabegalov, K.N., De Abreu, M.S., Gerasimova, E.V., Kalueff, A.V., 2022. Towards Zebrafish Models of CNS Channelopathies. Int. J. Mol. Sci. 23, 13979. https://doi.org/10.3390/ijms232213979

Li, J., Nelis, M., Sourbron, J., Copmans, D., Lagae, L., Cabooter, D., De Witte, P.A.M., 2021. Efficacy of Fenfluramine and Norfenfluramine Enantiomers and Various Antiepileptic Drugs in a Zebrafish Model of Dravet Syndrome. Neurochem. Res. 46, 2249–2261. https://doi.org/10.1007/s11064-021-03358-2

Livak, K.J., Schmittgen, T.D., 2001. Analysis of Relative Gene Expression Data Using Real-Time Quantitative PCR and the 2−ΔΔCT Method. Methods 25, 402–408. https://doi.org/10.1006/meth.2001.1262

Marini, C., Romoli, M., Parrini, E., Costa, C., Mei, D., Mari, F., Parmeggiani, L., Procopio, E., Metitieri, T., Cellini, E., Virdò, S., De Vita, D., Gentile, M., Prontera, P., Calabresi, P., Guerrini, R., 2017. Clinical features and outcome of 6 new patients carrying de novo *KCNB1* gene mutations. Neurol. Genet. 3, e206. https://doi.org/10.1212/NXG.0000000000000206

Mohapatra, D.P., Misonou, H., Sheng-Jun, P., Held, J.E., Surmeier, D.J., Trimmer, J.S., 2009. Regulation of intrinsic excitability in hippocampal neurons by activity-dependent modulation of the K_V 2.1 potassium channel. Channels 3, 46–56. https://doi.org/10.4161/chan.3.1.7655

Ogungbemi, A.O., Teixido, E., Massei, R., Scholz, S., Küster, E., 2021. Automated measurement of the spontaneous tail coiling of zebrafish embryos as a sensitive behavior endpoint using a workflow in KNIME. MethodsX 8, 101330. https://doi.org/10.1016/j.mex.2021.101330

Orellana-Paucar, A.M., Afrikanova, T., Thomas, J., Aibuldinov, Y.K., Dehaen, W., De Witte, P.A.M., Esguerra, C.V., 2013. Insights from Zebrafish and Mouse Models on the Activity and Safety of Ar-Turmerone as a Potential Drug Candidate for the Treatment of Epilepsy. PLoS ONE 8, e81634. https://doi.org/10.1371/journal.pone.0081634

Pena, I.A., Roussel, Y., Daniel, K., Mongeon, K., Johnstone, D., Weinschutz Mendes, H., Bosma, M., Saxena, V., Lepage, N., Chakraborty, P., Dyment, D.A., van Karnebeek, C.D.M., Verhoeven-Duif, N., Bui, T.V., Boycott, K.M., Ekker, M., MacKenzie, A., 2017. Pyridoxine-Dependent Epilepsy in Zebrafish Caused by Aldh7a1 Deficiency. Genetics 207, 1501–1518. https://doi.org/10.1534/genetics.117.300137

Raftery, T.D., Isales, G.M., Yozzo, K.L., Volz, D.C., 2014. High-Content Screening Assay for Identification of Chemicals Impacting Spontaneous Activity in Zebrafish Embryos.

Environ. Sci. Technol. 48, 804–810. https://doi.org/10.1021/es404322pupling. Neuron 31, 1035–1046. https://doi.org/10.1016/S0896-6273(01)00416-0

Saint-Amant, L., Drapeau, P., 1998. Time course of the development of motor behaviors in the zebrafish embryo. J. Neurobiol. 37, 622–632. https://doi.org/10.1002/(SICI)1097-4695(199812)37:4<622::AID-NEU10>3.0.CO;2-S

Saitsu, H., Akita, T., Tohyama, J., Goldberg-Stern, H., Kobayashi, Y., Cohen, R., Kato, M., Ohba, C., Miyatake, S., Tsurusaki, Y., Nakashima, M., Miyake, N., Fukuda, A., Matsumoto, N., 2015. De novo KCNB1 mutations in infantile epilepsy inhibit repetitive neuronal firing. Sci. Rep. 5, 15199. https://doi.org/10.1038/srep15199

Sakai, C., Ijaz, S., Hoffman, E.J., 2018. Zebrafish Models of Neurodevelopmental Disorders: Past, Present, and Future. Front. Mol. Neurosci. 11, 294. https://doi.org/10.3389/fnmol.2018.00294

Santos, D., Monteiro, S.M., Luzio, A., 2018. General Whole-Mount Immunohistochemistry of Zebrafish (Danio rerio) Embryos and Larvae Protocol, in: Félix, L. (Ed.), Teratogenicity Testing, Methods in Molecular Biology. Springer New York, New York, NY, pp. 365–371. https://doi.org/10.1007/978-1-4939-7883-0_19

Sarmiere, P.D., Weigle, C.M., Tamkun, M.M., 2008. The Kv2.1 K+ channel targets to the axon initial segment of hippocampal and cortical neurons in culture and in situ. BMC Neurosci. 9, 112. https://doi.org/10.1186/1471-2202-9-112

Scheldeman, C., Mills, J.D., Siekierska, A., Serra, I., Copmans, D., Iyer, A.M., Whalley, B.J., Maes, J., Jansen, A.C., Lagae, L., Aronica, E., de Witte, P.A.M., 2017. mTOR-related neuropathology in mutant tsc2 zebrafish: Phenotypic, transcriptomic and pharmacological analysis. Neurobiol. Dis. 108, 225–237. https://doi.org/10.1016/j.nbd.2017.09.004

Shen, H., Bocksteins, E., Kondrychyn, I., Snyders, D., Korzh, V., 2016. Functional antagonism of alpha-subunits of Kv channel in developing brain ventricular system. Development dev.140467. https://doi.org/10.1242/dev.140467

Shin, J.-N., Lee, K.-B., Butterworth, W., Park, S.-K., Kim, J.-Y., Kim, S., 2022. Zebrafish EEG predicts the efficacy of antiepileptic drugs. Front. Pharmacol. 13, 1055424. https://doi.org/10.3389/fphar.2022.1055424

Siekierska, A., Stamberger, H., Deconinck, T., Oprescu, S.N., Partoens, M., Zhang, Y., Sourbron, J., Adriaenssens, E., Mullen, P., Wiencek, P., Hardies, K., Lee, J.-S., Giong, H.-K., Distelmaier, F., Elpeleg, O., Helbig, K.L., Hersh, J., Isikay, S., Jordan, E., Karaca, E., Kecskes, A., Lupski, J.R., Kovacs-Nagy, R., May, P., Narayanan, V., Pendziwiat, M., Ramsey, K., Rangasamy, S., Shinde, D.N., Spiegel, R., Timmerman, V., Von Spiczak, S., Helbig, I., C4RCD Research Group, Balak, C., Belnap, N., Claasen, A., Courtright, A., De Both, M., Huentelman, M.J., Naymik, M., Richholt, R., Siniard, A.L., Szelinger, S., Craig, D.W., Schrauwen, I., AR working group of the EuroEPINOMICS RES Consortium, Afawi, Z., Balling, R., Baulac, S., Barišić, N., Caglayan, H.S., Craiu, D., Guerrero-López, R., Guerrini, R., Hjalgrim, H., Jähn, J., Klein, K.M., Leguern, E., Lemke, J.R., Lerche, H., Marini, C., Møller, R.S., Muhle, H., Rosenow, F., Serratosa, J., Suls, A., Stephani, U., Štěrbová, K., Striano, P., Zara, F., Weckhuysen, S., Francklyn, C., Antonellis, A., De Witte, P., De Jonghe, P., 2019a. Biallelic VARS variants cause developmental encephalopathy with microcephaly that is recapitulated in vars knockout zebrafish. Nat. Commun. 10, 708. https://doi.org/10.1038/s41467-018-07953-w

Siekierska, A., Stamberger, H., Deconinck, T., Oprescu, S.N., Partoens, M., Zhang, Y., Sourbron, J., Adriaenssens, E., Mullen, P., Wiencek, P., Hardies, K., Lee, J.-S., Giong, H.-K., Distelmaier, F., Elpeleg, O., Helbig, K.L., Hersh, J., Isikay, S., Jordan, E.,

Karaca, E., Kecskes, A., Lupski, J.R., Kovacs-Nagy, R., May, P., Narayanan, V., Pendziwiat, M., Ramsey, K., Rangasamy, S., Shinde, D.N., Spiegel, R., Timmerman, V., Von Spiczak, S., Helbig, I., C4RCD Research Group, Balak, C., Belnap, N., Claasen, A., Courtright, A., De Both, M., Huentelman, M.J., Naymik, M., Richholt, R., Siniard, A.L., Szelinger, S., Craig, D.W., Schrauwen, I., AR working group of the EuroEPINOMICS RES Consortium, Afawi, Z., Balling, R., Baulac, S., Barišić, N., Caglayan, H.S., Craiu, D., Guerrero-López, R., Guerrini, R., Hjalgrim, H., Jähn, J., Klein, K.M., Leguern, E., Lemke, J.R., Lerche, H., Marini, C., Møller, R.S., Muhle, H., Rosenow, F., Serratosa, J., Suls, A., Stephani, U., Štěrbová, K., Striano, P., Zara, F., Weckhuysen, S., Francklyn, C., Antonellis, A., De Witte, P., De Jonghe, P., 2019b. Biallelic VARS variants cause developmental encephalopathy with microcephaly that is recapitulated in vars knockout zebrafish. Nat. Commun. 10, 708. https://doi.org/10.1038/s41467-018-07953-w

Speca, D.J., Ogata, G., Mandikian, D., Bishop, H.I., Wiler, S.W., Eum, K., Wenzel, H.J., Doisy, E.T., Matt, L., Campi, K.L., Golub, M.S., Nerbonne, J.M., Hell, J.W., Trainor, B.C., Sack, J.T., Schwartzkroin, P.A., Trimmer, J.S., 2014. Deletion of the Kv2.1 delayed rectifier potassium channel leads to neuronal and behavioral hyperexcitability: Kv2.1 deletion and hyperexcitability. Genes Brain Behav. 13, 394–408. https://doi.org/10.1111/gbb.12120

Suo, G., Cao, X., Zheng, Y., Li, H., Zhang, Q., Tang, J., Wu, Y., 2021. A de novo nonsense mutation of STXBP1 causes early-onset epileptic encephalopathy. Epilepsy Behav. 123, 108245. https://doi.org/10.1016/j.yebeh.2021.108245

Swaminathan, A., Hassan-Abdi, R., Renault, S., Siekierska, A., Riché, R., Liao, M., de Witte, P.A.M., Yanicostas, C., Soussi-Yanicostas, N., Drapeau, P., Samarut, É., 2018. Non-

canonical mTOR-Independent Role of DEPDC5 in Regulating GABAergic Network Development. Curr. Biol. 28, 1924-1937.e5. https://doi.org/10.1016/j.cub.2018.04.061

Thiffault, I., Speca, D.J., Austin, D.C., Cobb, M.M., Eum, K.S., Safina, N.P., Grote, L., Farrow, E.G., Miller, N., Soden, S., Kingsmore, S.F., Trimmer, J.S., Saunders, C.J., Sack, J.T., 2015. A novel epileptic encephalopathy mutation in KCNB1 disrupts Kv2.1 ion selectivity, expression, and localization. J. Gen. Physiol. 146, 399–410. https://doi.org/10.1085/jgp.201511444

Tiraboschi, E., Martina, S., Ent, W., Grzyb, K., Gawel, K., Cordero-Maldonado, M.L., Poovathingal, S.K., Heintz, S., Satheesh, S.V., Brattespe, J., Xu, J., Suster, M., Skupin, A., Esguerra, C.V., 2020. New insights into the early mechanisms of epileptogenesis in a zebrafish model of Dravet syndrome. Epilepsia 61, 549–560. https://doi.org/10.1111/epi.16456

Torkamani, A., Bersell, K., Jorge, B.S., Bjork, R.L., Friedman, J.R., Bloss, C.S., Cohen, J., Gupta, S., Naidu, S., Vanoye, C.G., George, A.L., Kearney, J.A., 2014. De novo KCNB1 mutations in epileptic encephalopathy: KCNB1 Mutations. Ann. Neurol. 76, 529–540. https://doi.org/10.1002/ana.24263

Trimmer, J.S., 1991. Immunological identification and characterization of a delayed rectifier K+ channel polypeptide in rat brain. Proc. Natl. Acad. Sci. 88, 10764–10768. https://doi.org/10.1073/pnas.88.23.10764

Vierra, N.C., Kirmiz, M., van der List, D., Santana, L.F., Trimmer, J.S., 2019. Kv2.1 mediates spatial and functional coupling of L-type calcium channels and ryanodine receptors in mammalian neurons. eLife 8, e49953. https://doi.org/10.7554/eLife.49953

Vliet, S.M.F., Dasgupta, S., Sparks, N.R.L., Kirkwood, J.S., Vollaro, A., Hur, M., Zur Nieden, N.I., Volz, D.C., 2019. Maternal-to-zygotic transition as a potential target for

niclosamide during early embryogenesis. Toxicol. Appl. Pharmacol. 380, 114699. https://doi.org/10.1016/j.taap.2019.114699

Whyte-Fagundes, P.A., Vance, A., Carroll, A., Figueroa, F., Manukyan, C., Baraban, S.C., 2024. Testing of putative antiseizure medications in a preclinical Dravet syndrome zebrafish model. Brain Commun. 6, fcae135. https://doi.org/10.1093/braincomms/fcae135

Winter, M.J., Pinion, J., Tochwin, A., Takesono, A., Ball, J.S., Grabowski, P., Metz, J., Trznadel, M., Tse, K., Redfern, W.S., Hetheridge, M.J., Goodfellow, M., Randall, A.D., Tyler, C.R., 2021. Functional brain imaging in larval zebrafish for characterising the effects of seizurogenic compounds acting via a range of pharmacological mechanisms. Br. J. Pharmacol. 178, 2671–2689. https://doi.org/10.1111/bph.15458

Yaksi, E., Jamali, A., Diaz Verdugo, C., Jurisch-Yaksi, N., 2021. Past, present and future of zebrafish in epilepsy research. FEBS J. 288, 7243–7255. https://doi.org/10.1111/febs.15694

Zhang, Y., Kecskés, A., Copmans, D., Langlois, M., Crawford, A.D., Ceulemans, B., Lagae, L., de Witte, P.A.M., Esguerra, C.V., 2015. Pharmacological Characterization of an Antisense Knockdown Zebrafish Model of Dravet Syndrome: Inhibition of Epileptic Seizures by the Serotonin Agonist Fenfluramine. PLOS ONE 10, e0125898. https://doi.org/10.1371/journal.pone.0125898

Figure legends

Figure 1. Expression of kcnb1 in the Diencephalon, Midbrain, and Hindbrain of Wild-type larval zebrafish. A and B. Horizontal and transversal sections of Wild-type (WT) zebrafish expressing cells (DAPI, blue) labelled with anti-kcnb1 (green), showing a large

expression of the protein in the central nervous system (CNS) at 6-day post-fertilization (dpf). The protein is mainly expressed in the Diencephalon region, in the Midbrain region including the optic tectum, and in the Hindbrain region comprising the cerebellum and in the spinal cord. However, the protein was not found in the Telecephalon of the horizontal section (scale bar: 50 µm; magnification: 10x and 20x). CNS regions are delimited by dotted lines. **C.** Horizontal section of a WT zebrafish at 6 dpf showing the presence of kcnb1 along the spinal cord (scale bar: 20 µm; magnification: 63x). **D.** Zoom at 63x magnification of the brain horizontal section showing the expression of kcnb1 at the cell surface and seemingly following the shape of the soma in the diencephalon region (scale bar: 20 µm; magnification: 63x). n = 3 fish/section; D: Diencephalon; DAPI: 4,6-diamidino-2-phenylindole; H: Hindbrain; M: Midbrain; T: Telencephalon.

Figure 2. Genotypic characterization of a *kcnb1* knock-out zebrafish model. A. Schematic illustration of the generation of a *kcnb1* knock-out zebrafish model obtained by Shen et al. (2016). The representation of the α-subunit *kcnb1* is adapted from Hermann et al. (2015). Insertion of a 14 base-pairs (bp)-nucleotide sequence (identified in red) and of a 2 bp-nucleotide deleted (identified in black bold type) into the first exon of the gene introducing a premature stop (Δ14bp) between the N-terminal region and the first transmembrane domain of the protein, using the CRISPR-Cas9 system (targeted sequence: GGAGCTGGACTACTGGGGAG in *kcnb1* exon 1; ID zfin: ZDB-ALT-170417-2; indel mutation; line: $Kcnb1^{sq301/sq301}$). **B.** Identification of a melting curve shift due to DNA mutations in $kcnb1^{+/-}$ and $kcnb1^{-/-}$ compared with $kcnb1^{+/+}$ fish and obtained by High Resolution Melting Analysis (HRMA). **C.** RT-qPCR analysis of total *kcnb1* at 6 dpf demonstrating a significant decrease of *kcnb1* mRNA in $kcnb1^{+/-}$ and $kcnb1^{-/-}$ compared with $kcnb1^{+/+}$ fish ($kcnb1^{+/+}$ = 1 ± 0 arbitrary unit (AU); $kcnb1^{+/-}$ = 0.56 ± 0.096 AU; $kcnb1^{-/-}$ = 0.44 ± 0.084 AU; +/+ *vs* mutants: $p<0.01$; N = 4; n = 30/sample; Mann-

Withney test; **p<0,01). Data are normalized to actin mRNA expression and the condition *kcnb1*$^{+/+}$ is considered as the reference value (relative fold change = 1). Values represent the mean ± standard error of the mean (SEM). **D.** Transversal sections of control and *kcnb1* knock-out zebrafish models expressing cells (DAPI, blue) labelled with anti-kcnb1 (red) at 6 dpf, showing a loss of kcnb1 protein expression in the CNS of mutant fish. The CNS region is delimited by dotted lines (n = 3 fish/genotype; scale bar: 50 µm; magnification: 20x). **E.** Kaplan-Meier survival curve between 0 and 15 dpf showing that the partial or complete loss of *kcnb1* do not impact the normal growth of fish at early stages of development (see **Figure 2-table 2**; N = 3 repeats; n = 121-169/genotype; Log-rank test; +/+ *vs* mutants: p>0.5; ns: non-significant). For all experiments, at least 3 individual experiments were realized (N) with a certain number of fish (n).

Figure 3. *kcnb1* loss of function led to early behavioral phenotype deficiency. A. Locomotor activity heatmap reflecting the **(Figure 3B)** average number of movements per minute of embryos in their chorion between 24 hpf and 36 hpf. A significant decrease in general spontaneous movements (coiling and twitching) of *kcnb1* mutant models (*kcnb1*$^{+/-}$ and *kcnb1*$^{-/-}$) was observed as compared to the WT condition (*kcnb1*$^{+/+}$) (see **Figure 3-figure supplement 1** and **Figure 3-video 1A-C**; tail coiling number at 25 hpf: *kcnb1*$^{+/+}$ = 2.98 ± 0.20; *kcnb1*$^{+/-}$ = 2.12 ± 0.108; *kcnb1*$^{-/-}$ = 2.07 ± 0.18; +/+ *vs* mutants: p<0.01; tail coiling number at 31 hpf: *kcnb1*$^{+/+}$ = 0.52 ± 0.83; *kcnb1*$^{+/-}$ = 0.13 ± 0.036; *kcnb1*$^{-/-}$ = 0.14 ± 0.04; +/+ *vs* mutants: p<0.0001; N = 3 repeats; n = 80-104 ZF/genotype; one-way ANOVA with Bonferroni post-hoc test; ns: non-significant; *p<0,05; **p<0,01; ****p<0,0001). Values represent the mean ± standard error of the mean (SEM). **C.** Representative traces of individual swimming episodes at 48 hpf showing the typical tortuous trajectory of *kcnb1* mutant models (*kcnb1*$^{+/-}$ and *kcnb1*$^{-/-}$) as compared to the straight-line trajectory of *kcnb1*$^{+/+}$ fish (5 trajectories/genotype). **D-F.** The

quantification of the swimming trajectory tortuosity shows a significant increase of different studied parameters in both *kcnb1* mutant conditions (*kcnb1*$^{+/-}$ and *kcnb1*$^{-/-}$) as compared to control fish (*kcnb1*$^{+/+}$), including an increase of the distance swam **(Figure 3D)**, the velocity **(Figure 3E)** and the time spent in motion **(Figure 3F)**. Furthermore, within the same genotype, a huge variability in the swimming behavior has been observed and fish were divided into two distinct phenotypes: severe (SP; at least two swim circles) and mild (MP; other trajectories). The subdivision of both phenotypes is represented in Figure 3-**table 3** and **Figure 3-figure supplement 2** (see **Figure 3-video 2A-B**; distance swam: *kcnb1*$^{+/+}$ = 57.75 ± 4.23 mm; *kcnb1*$^{+/-}$ = 100.26 ± 7.13 mm; *kcnb1*$^{-/-}$ = 93.8 ± 7.10 mm; +/+ *vs* mutants: p<0.0001; N = 3 repeats; n = 50-88 ZF/genotype; one-way ANOVA with Bonferroni post-hoc test; ns: non-significant; *p<0,05; **p<0,01; ***p<0,001; ****p<0,0001). Values represent the mean ± standard error of the mean (SEM).

Figure 4. *kcnb1* knock-out zebrafish model displayed light and sound-induced locomotor activity impairments during larvae stages. A. Schematic representation of individual trajectory of 3 larvae zebrafish per genotype obtained with ViewPoint software (Zebrabox). Between 3 and 6 dpf, a protocol was applied to fish with 3 repetitions of 10 minutes in the light followed by 10 minutes in the dark (green lines: slow movements <8 mm/sec; red lines: fast movements >8 mm/sec; see **Figure 4-video 3**). **B.** Average distance swam by larvae zebrafish at 6 dpf during the whole light-dark protocol described previously. Spontaneous locomotor hyperactivity was observed in *kcnb1*$^{-/-}$ larvae in the light and maintained significantly increased during the dark phase as compared to WT and *kcnb1*$^{+/-}$ larvae (N = 3 repeats; n = 35 ZF/genotype; two-ways ANOVA with Bonferroni post-hoc test; *p<0,05; **p<0,01; ***p<0,001; ****p<0,0001). Values represent the mean ± standard error of the mean (SEM). **C.** Representation of average distance travelled by larvae at different early days of development

(from 3 to 6 dpf) following the 10 min light-dark protocol described. At 3 and 4 dpf, controls and *kcnb1* mutant fish (*kcnb1*$^{+/-}$ and *kcnb1*$^{-/-}$) present low locomotor activity that was significantly increased from 5 to 6 dpf. A significant gap was observed starting from 5 dpf with a locomotor hyperactivity for *kcnb1*$^{-/-}$ larvae as compared to WT and *kcnb1*$^{+/-}$ fish, reflecting the result obtained in **Figure 4B** (distance at 6 dpf: *kcnb1*$^{+/+}$ = 3.98 ± 0.43 cm; *kcnb1*$^{+/-}$ = 3.42 ± 0.54 cm; *kcnb1*$^{-/-}$ = 8.29 ± 0.76 cm; +/+ *vs* -/- : p<0.0001; N = 3 repeats; n = 35 ZF/genotype; two-ways ANOVA with Bonferroni post-hoc test; the locomotor activity of fish from the same genotype was compared from 4 to 6 dpf with a reference value at 3 dpf and the three genotypes were also compared between them; ns: non-significant; *p<0,05; **p<0,01; ***p<0,001; ****p<0,0001). Values represent the mean ± standard error of the mean (SEM). **D.** Quantification of the distance swam during the 5 seconds following each of the four sound stimulations applied (450 Hertz; 80 decibels; 1 second) to larvae at 6 dpf. Both mutant conditions (*kcnb1*$^{+/-}$ and *kcnb1*$^{-/-}$) present a significant decrease of the locomotor activity in response to the sound stimulations as compared to the control condition (+/+ *vs* mutants: p<0.5; N = 3 repeats; n = 48-64 ZF/genotype; one-way ANOVA with Bonferroni post-hoc test; *p<0,05). Values represent the mean ± standard error of the mean (SEM).

Figure 5. *kcnb1* knock-out zebrafish exhibited an increase of sensitivity due to PTZ-induced seizures and an increase of epileptogenesis-related *bdnf* gene expression at 6 dpf. **A.** Schematic representation of individual trajectory of 3 larvae zebrafish per genotype obtained with ViewPoint software (Zebrabox). Fast swimming circles were observed for both mutant larvae conditions (*kcnb1*$^{+/-}$ and *kcnb1*$^{-/-}$) after 30 minutes of Pentylenetetrazol (PTZ) treatment at 5 mM, a pro-convulsant. Green lines: slow movements (<8 mm/sec), red lines: fast movements (>8 mm/sec). **B.** Global locomotor activity of 6 dpf-zebrafish into the dark was recorded by applying a protocol of 30 minutes of basal activity followed by 30 minutes of

chemically induced-seizures using PTZ treatment at 5 mM. Both *kcnb1*$^{+/-}$ and *kcnb1*$^{-/-}$ larvae show a significant increase in distance travelled during the 30 min-recording after the chemical treatment as compared to wild-type fish (*kcnb1*$^{+/+}$) (distance at 60 min : *kcnb1*$^{+/+}$ = 8.59 ± 4.23 cm; *kcnb1*$^{+/-}$ = 40.9 ± 6.86 cm; *kcnb1*$^{-/-}$ = 37.9 ± 5.60 cm; +/+ *vs* mutants: p<0.0001; N = 3 repeats; n = 27 ZF/genotype; one-way ANOVA with Bonferroni post-hoc test; ns: non-significant; +/- and -/- *vs* +/+ after PTZ treatment: **p<0,01; ****p<0,0001). Values represent the mean ± standard error of the mean (SEM). **C.** RT-qPCR analysis of total *bdnf* at 6 dpf, a neurogenesis and epileptogenesis-related gene, before (*kcnb1*$^{+/+}$ = 1 ± 0 AU; *kcnb1*$^{+/-}$ = 2.28 ± 0.42 AU; *kcnb1*$^{-/-}$ = 3.01 ± 0.45 AU; +/+ *vs* mutants: p>0.5; N = 3; n = 30/sample; Mann-Whitney test; ns: non-significant) and after PTZ treatment at 5 mM (*kcnb1*$^{+/+}$ = 1.56 ± 0.27 AU; *kcnb1*$^{+/-}$ = 3.24 ± 1.24 AU; *kcnb1*$^{-/-}$ = 29.4 ± 6.99 AU; +/+ *vs* -/-: p<0.0001; N = 3; n = 30/sample; Mann-Whitney test; ****p<0,0001). Data are normalized to ef1α mRNA expression and *kcnb1*$^{+/+}$ non-treated fish are considered as the reference value (relative fold change = 1). The *kcnb1*$^{-/-}$ presents a tendency to an increased bdnf expression during the basal locomotor activity which is confirmed by a significant increased expression after chemically induced-seizures as compared to *kcnb1*$^{+/+}$ *and kcnb1*$^{+/-}$. Values represent the mean ± standard error of the mean (SEM). **D.** Whole-mount images of 6 dpf-zebrafish immunostained with anti-c-Fos, an acute neuronal activation marker, obtained 30 minutes after a basal activity period and a provoked-seizures period due to PTZ treatment at 5 mM. The telencephalon was the major region activated after the chemical treatment for each genotype (n = 8-11 ZF/condition, dorsal view, 3D reconstruction, scale bar: 50 µm, magnification 20x). **E.** Quantification of the number of c-Fos positive neurons normalized to the volume (µm^3) of the telencephalon of 6 dpf larvae-zebrafish during their basal activity or chemically treated using the software IMARIS. The results did not show any difference in the number of activated neurons reflected by c-Fos fluorescence intensity in the telencephalon of both mutant conditions (*kcnb1*$^{+/-}$ and *kcnb1*$^{-/-}$) as

compared to the WT condition (see **Figure 5-figure supplement 3A**; +/+ *vs* mutants: p>0.5; n = 8-11 fish/condition; Mann-Whitney test; ns: non-significant). Values represent the mean ± standard error of the mean (SEM). **F.** Distribution (in %) of activated neurons according to the fluorescence intensity value of c-Fos in the telencephalon of fish at 6 dpf, reflecting the level of neuronal activation that was divided in four equal shares (from 0 to 100%): low (0-25%), moderately low (25-50%), moderately high (50-75%) and high (75-100%) neuronal activation. The three non-treated conditions were presenting a similar distribution with a majority of low neuronal activation of c-Fos positive neurons. However, chemically treated *kcnb1*$^{-/-}$ fish were presenting a global higher activation with a significant shift to a moderately low and moderately high neuronal activation (see **Figure 5-figure supplement 3B**; +/+ *vs* -/-: p<0.5; n = 8-11 fish/condition; Mann-Whitney test; *p<0,05). bdnf: Brain-Derived Neurotrophic Factor; T: Telencephalon. Values represent the mean ± standard error of the mean (SEM).

Figure 6. *kcnb1* knock-out zebrafish models present increased provoked-epileptic seizures at 5 dpf. A. Schematic representation of the protocol applied for electroencephalographic recordings of 5 dpf-zebrafish. Neuronal activity in the optic tectum of zebrafish was recorded by applying a protocol of 30 minutes of basal activity followed by 30 minutes of PTZ treatment at 40 mM. 10 minutes in the middle of each period (basal activity and provoked seizures) was used to analyze the total number of negative spikes of each genotype. **B.** Representative traces of electroencephalographic recordings in the optic tectum for control and *kcnb1* knock-out larvae showing variations in the recorded electrical activity and polyspike discharges in the *kcnb1*$^{-/-}$ model. **C.** Quantification of electrophysiological recordings by analyzing the total number of negative spikes over 10 minutes of each basal activity and provoked-seizures periods as described in **Figure 6A**. Results show a significant increase of neuronal activity in the *kcnb1*$^{+/-}$ and *kcnb1*$^{-/-}$ models after a PTZ treatment at 40 mM as compared to the same genotype

without treatment (see **Figure 6-table 4**; n = 3-5 ZF/genotype; Mann-Whitney test, *p<0,05; **p<0,01). Values represent the mean ± standard error of the mean (SEM).

Figure 7. *kcnb1* mutant zebrafish models are not affected by global morphological alterations or brain anatomical defects. A. Images showing that *kcnb1*$^{+/-}$ and *kcnb1*$^{-/-}$ embryos and larvae do not show gross morphological changes at 28 hours post-fertilization (hpf) and 6 dpf (scale bar: 300 µm). **B.** Quantification of major morphological aspects at 48 hpf and 6 dpf including measurement of body length and head surface. The *kcnb1* mutant zebrafish models (*kcnb1*$^{+/-}$ and *kcnb1*$^{-/-}$) do not show any significant change in each parameter at different developmental stages as compared to *kcnb1*$^{+/+}$ (see **Figure 7-figure supplement 4**; body length at 6 dpf: *kcnb1*$^{+/+}$ = 3.45 ± 0.03 mm; *kcnb1*$^{+/-}$ = 3.82 ± 0.02 mm; *kcnb1*$^{-/-}$ = 3.62 ± 0.04 mm; +/+ *vs* mutants: p>0.5; N = 4 repeats; n = 28-38 ZF/genotype; one-Way ANOVA with Bonferroni post-hoc test; ns: non-significant). Values represent the mean ± standard error of the mean (SEM). **C.** Transversal slices of 48 hpf and 4 dpf larvae expressing cells (DAPI, blue) labelled with anti-HuC (red), a pan-neuronal marker, showing no major difference of anatomical brain regions between mutants and wild-type fish (scale bar: 50 µm; magnification 20x). **D and E.** Whole-mount images of embryonic (48 hpf) and larvae (6 dpf) zebrafish immunostained with **(D)** anti-3A10 marker to identify Mauthner cells (see **Figure 7-figure supplement 5**; dorsal view; 3D reconstruction; scale bar: 50 µm; magnification 20x) and **(E)** anti-acetylated tubulin marker to identify global circuits of neuronal fibers (lateral and dorsal view; 3D reconstruction; magnification 20x and scale bar at 50 µm; magnification 40x and scale bar at 20 µm). The partial or complete loss of *kcnb1* does not affect the neuronal brain density at different early stages of development (n = 5-7 ZF/genotype/developmental stage).

Figure 8. *kcnb1* loss-of-function causes neurotransmission defects at the neuromuscular junctions (NMJ) but no alteration of muscle and NMJ organization. A. Whole-mount images of 48 hpf-zebrafish obtained with a brightfield microscopy and treated with Phalloidin preventing actin depolymerization to identify general muscle fiber organization **(Figure 8A*a* and 8A*b*)**. Fish were then labelled with anti-F310 and anti-F59 markers to differentiate, respectively, fast and slow muscle fibers **(Figure 8A*c* and 8A*d*)**. Control fish (*kcnb1*$^{+/+}$) and *kcnb1* mutant models (*kcnb1*$^{+/-}$ and *kcnb1*$^{-/-}$) display well organized muscle structures with typical parallel line pattern at 48 hpf (n = 4-8 ZF/genotype; 3D reconstruction; lateral view; magnification 20x; scale bar: 50 µm). **B.** Quantification of the anisotropy of fibrillar structures in raw images of Phalloidin, F310 and F59 labelling using the plugin FibrilTool from the software ImageJ (Boudaoud et al., 2014). A Gaussian filter was applied on images and the anisotropy was analyzed reflecting the organization of fibers following the convention: 0 for no order and 1 for perfectly ordered (parallel fibrils) (anisotropy of fast muscles (F310): *kcnb1*$^{+/+}$ = 0.443 ± 0.02; *kcnb1*$^{+/-}$ = 0.387 ± 0.06; *kcnb1*$^{-/-}$ = 0.51 ± 0.02; +/+ *vs* mutants: p>0.5; n = 5-12 ZF/genotype/marker; Mann-Whitney test; ns: non-significant). Values represent the mean ± standard error of the mean (SEM). **C.** Plot profile illustrating the relative distance between fibers for each muscle fibers labelling (Phalloidin, F310 and F59). The results show similar profiles between control and both mutant conditions reflecting well organized muscle fibers (n = 4-8 ZF/genotype/marker). **D.** Primary motoneuron axons of controls and *kcnb1* mutant zebrafish at 48 hpf were immunostained with anti-Znp1 marker (green) and acetylcholine receptors (AchR) were labelled with Bungarotoxin (BTX, red) (n = 4-8 ZF/genotype, magnification 20x, scale bar: 50 µm). At 48 hpf, to ef1α mRNA expression and *kcnb1*$^{+/+}$ fish are considered as the reference value (relative mutant fish (*kcnb1*$^{+/-}$ and *kcnb1*$^{-/-}$) present similar motor axons length and branching as compared to WT fish associated with colocalization with AchR puncta identified along axons, quantified with Imaris software and represented by yellow

spots, indicating functional synapses. **E.** Quantification of motor axon length of fish at 48 hpf. An average of eight motor axon length per fish was measured and a ratio was applied according to the spinal cord thickness. The total length quantification did not show any difference in motor axon size between mutant zebrafish models and the control condition (*kcnb1*$^{+/+}$ = 2.38 ± 0.11; *kcnb1*$^{+/-}$ = 2.43 ± 0.06; *kcnb1*$^{-/-}$ = 2.55 ± 0.14; +/+ *vs* mutants: p>0.5; n = 7–9 ZF/condition; Mann-Whitney test; ns: non-significant). Values represent the mean ± standard error of the mean (SEM). **F and G.** Total RNAs were extracted from fish at 6 dpf and RT-PCR was performed to determine the transcript level of **(F)** acetylcholinesterase (AchE) and of **(G)** subunits α1, γ, ε (chrn) of AchR. Data are normalized to ef1α mRNA expression and the condition *kcnb1*$^{+/+}$ is considered as the reference value (relative fold change = 1). Both mutant conditions (*kcnb1*$^{+/-}$ and *kcnb1*$^{-/-}$) presented significant decrease of AchE expression, reflecting a neurotransmission recycling defect at the NMJ level **(Figure 8F)**. However, the composition of AchR subunits is similar between conditions **(Figure 8G)**. N = 3; n = 30/sample; Mann-Whitney test; ns: non-significant; *p<0,05; **p<0,01. Values represent the mean ± standard error of the mean (SEM). chrn: cholinergic receptor nicotinic.

Tables

Gene	Forward primer	Reverse primer
β-actin	5'-CGAGCTGTCTTCCCATCCA-3'	5'-TCACCAACGTAGCTGTCTTTCTG-3'
ef1α	5'-CTGGAGGCCAGCTCAAACAT-3'	5'-ATCAAGAAGAGTAGTACCGCTAGCATTAC-3'
kcnb1	5'-TGAAGTTCCGGGAGAGTGTT-3'	5'-CAGGTTGGCGATGTCGTTCT-3'
bdnf	5'-GACTCGAAGGACGTTGACCTGTA-3'	5'-CGGCTCCAAAGGCACTTG-3'
achE	5'-GAACCTGAAGCCCTTAGAGG-3'	5'-TCGTCCAGAGTATCGGTGG-3'

chrn γ	5'-GACACCTGAGCAGGAGGAAG-3'	5'-GGACACACACTGCTGCACTT-3'
chrn ε	5'-TAGTTGCTATTGTGCTTCTG-3'	5'-CTCTTCATTCCCAGTGACTT-3'
chrn α1	5'-TCGTCCTGTTAGCCATTTTA-3'	5'-GATTAACTTCATCCACGCTG-3'

Table 1: List of primers used for RT-qPCR.

Conditions	**Number of alive fish**		**% survival (0 vs 15 dpf)**	**Log-rank test at 15 dpf (mutant vs WT)**
	0 dpf	**15 dpf**		
***kcnb1*$^{+/+}$**	**137**	**116**	**84,67**	**/**
***kcnb1*$^{+/-}$**	**121**	**109**	**82,65**	**P = 0,7677**
***kcnb1*$^{-/-}$**	**169**	**156**	**88,17**	**P = 0,3302**

Figure 2-table 2: Survival table between 0 and 15 days post-fertilization (dpf). Results show a similar growth of *kcnb1* mutant fish (*kcnb1*$^{+/-}$ and *kcnb1*$^{-/-}$) as compared to control fish (*kcnb1*$^{+/+}$) at early stages development (N = 3 repeats; n = 121-169 ZF/genotype, Logrank test, ns: non-significant).

	Total number of embryos	**Mild phenotype**	*** Severe phenotype**	**% Severe phenotype**
***kcnb1*$^{+/+}$**	73	/	/	/
***Kcnb1*$^{+/-}$**	88	61	27	30,68%
***kcnb1*$^{-/-}$**	50	24	26	52%

Figure 3-table 3: Diverse phenotypes were observed during the Touch-Evoked Escape Response (TEER) of 48 hpf-mutant embryos. Embryos with the same genotype were divided

in severe phenotype (* : locomotion with a trajectory of at least two swim circles; SP) and mild phenotype (other trajectories; MP) indicating a huge variability in swimming behavior in the same condition after a TEER test of *kcnb1*$^{+/-}$ and *kcnb1*$^{-/-}$ fish (N = 3 repeats; n = 50-88 ZF/genotype).

Condition	***kcnb1* +/+**			***kcnb1* +/-**					***kcnb1* -/-**			
Animal	1	2	3	1	2	3	4	5	1	2	3	4
Age (dpf)	5	5	5	5	5	5	5	5	5	5	5	5
Duration of recording/period (min)	10	10	10	10	10	10	10	10	10	10	10	10
Number of all spikes in basal activity	214	167	134	192	307	123	116	8	410	85	79	450
Number of all spikes after PTZ [40mM] treatment	1643	926	1002	3690	1991	1211	5515	1600	2230	941	500	1313

Figure 6-table 4: Individual data of negative spikes number during electrophysiological recordings into the optic tectum of zebrafish at 5 dpf. The neuronal activity of fish was recorded during 30 minutes of basal activity followed by 30 minutes of PTZ treatment at 40 mM. A period of 10 minutes in the middle of each period (basal activity and provoked seizures) was used to analyze the number of spikes. The table shows a higher number of negative spikes for each *kcnb1*$^{+/-}$ and *kcnb1*$^{-/-}$ models after PTZ treatment as compared to non-treated fish but shows also a huge variability between fish from the same genotype. The following parameters were applied for each recording: Resistance: 5-10 mΩ; Lowpass: Gaussian 560 Hz; Data reduction: 10; Min allowed duration: 10; Negative ongoing analysis. n = 3-5 ZF/genotype.

Figure supplements

Figure 3-figure supplement 1: *kcnb1* mutant zebrafish models present premotor hypoactivity during the first hours of development. Average number of tail movements per minute of embryos in their chorion at 26 hpf illustrating a decrease in general spontaneous movement (coiling and twitching) of *kcnb1* mutant models (*kcnb1*$^{+/-}$ and *kcnb1*$^{-/-}$) as compared to wild-type fish (*kcnb1*$^{+/+}$) (tail coiling number: *kcnb1*$^{+/+}$ = 3.21 ± 0.17; *kcnb1*$^{+/-}$ = 1.48 ± 0.098; *kcnb1*$^{-/-}$ = 1.75 ± 0.14; +/+ *vs* mutants: p<0.001; N = 3 repeats; n = 86-94 ZF/genotype; one-way ANOVA with Bonferroni post-hoc test; ****p<0,0001). Values represent the mean ± standard error of the mean (SEM).

Figure 3-figure supplement 2: *kcnb1* mutant zebrafish models present a variability in the swimming behavior at 48 hpf. A. Within the same genotype, the swimming behavior of fish has been divided into two distinct phenotypes: severe (at least two swim circles, severe phenotype, SP) and mild (other trajectories, mild phenotype, MP) during the 2nd dpf. The subdivision of both swimming behavior (severe and mild phenotype) per genotype is represented as traces of individual swimming episodes showing a huge variability of trajectories (4 trajectories/phenotype). 30,68% of *kcnb1*$^{+/-}$ fish and 52% of *kcnb1*$^{-/-}$ fish were identified with a severe phenotype (see **Figure 3-table 3**). **B.** The variability between both swimming phenotypes was quantified following different parameters including the distance swam, the velocity and the time spent in motion. The results show similar values between both mutant conditions presenting a mild phenotype as compared to the control condition (*kcnb1*$^{+/+}$). Nevertheless, fish with a severe phenotype present a significant increase of the studied parameters for both genotypes (*kcnb1*$^{+/-}$ and *kcnb1*$^{-/-}$). distance swam: p(+/+ *vs* +/- MP)>0.5; p(+/+ *vs* +/- SP)<0.0001; p(+/+ *vs* -/- MP)>0.5; p(+/+ *vs* -/- SP)<0.0001; N = 3 repeats; n = 50-88 ZF/genotype; one-way ANOVA with Bonferroni post-hoc test; **p<0,01; ***p<0,001; ****p<0,0001. Values represent the mean ± standard error of the mean (SEM).

Figure 5-figure supplement 3: Shift of c-Fos positive-neuron intensity distribution from a global low neuronal activation to a higher neuronal activation in the telencephalon region of *kcnb1*$^{-/-}$ fish at 6 dpf after chemically provoked-seizures. A. Whole larvae-fish at 6 dpf were fixed 30 minutes after a basal activity period and a provoked-seizures period due to PTZ treatment at 5 mM followed by the labelling of c-Fos, an acute neuronal activation marker. The number of c-Fos positive-neurons and the fluorescence intensity value of c-Fos per neuron were quantified using the software IMARIS by analyzing the telencephalon, the major region activated after the chemical treatment. The contour of the region of interest has been designed manually to obtain the volume (µm^3) of the telencephalon, neurons were then identified automatically within the region following identical parameters for spot detection between conditions and visualized in 3 dimensions to avoid false negative spots. Values were normalized according to the volume of the telencephalon (see **Figure 5D-5F**; n = 8-11 fish/condition). **B.** Distribution (in %) of c-Fos positive-neurons according to the fluorescence intensity value of c-Fos in the telencephalon of fish at 6 dpf, reflecting the level of neuronal activation that was divided in four equal shares (from 0 to 100%): low (0-25%), moderately low (25-50%), moderately high (50-75%) and high (75-100%) neuronal activation. During the basal activity, the distribution of activated neurons is similar between each condition with a majority of neurons presenting a low neuronal activation. However, a shift to a moderately low and moderately high neuronal activation was observed for each condition after a PTZ treatment, with a global higher activation in the *kcnb1*$^{-/-}$ condition. n = 8-11 fish/condition; T: Telencephalon.

Figure 7-figure supplement 4: No major morphological malformation of *kcnb1* mutant models at embryonic and larval developmental stages. Quantification of major

morphological aspects including measurement of the **(A)** body surface, **(B)** head length, **(C-E)** eye diameter, surface and spacing, **(F)** swim bladder surface of embryonic (48 hpf) and larvae (6 dpf) zebrafish and of the **(G)** protruding-mouth length from 7 to 9 dpf. Both *kcnb1* knock-out zebrafish models do not present a developmental delay or major morphological changes as compared to *kcnb1*$^{+/+}$ fish. Only a significant decrease of the eye diameter was observed in *kcnb1*$^{-/-}$ fish at 48 hpf but recovered at 6 dpf with values similar to those obtained in *kcnb1*$^{+/+}$ and *kcnb1*$^{+/-}$ conditions (+/+ *vs* mutants: p>0.5; N = 3-4 repeats; n = 16-38 ZF/genotype; one-Way ANOVA with Bonferroni post-hoc test; ns: non-significant; ***p<0,001). Values represent the mean ± standard error of the mean (SEM).

Figure 7-figure supplement 5: Quantification of Mauthner cell body length of fish at 48 hpf. Fish were labelled with anti-3A10 and the length of Mauthner cell body (M-cell) was measured between the two extremities as represented with the arrow. The average value of the two M-cell bodies of each fish was used for quantification. Both *kcnb1* knock-out zebrafish models (*kcnb1*$^{+/-}$ and *kcnb1*$^{-/-}$) do not present difference in the length of M-cell body at 48 hpf as compared to the control condition (*kcnb1*$^{+/+}$). *kcnb1*$^{+/+}$ = 39.58 ± 2.26 µm; *kcnb1*$^{+/-}$ = 37.52 ± 0.86 µm; *kcnb1*$^{-/-}$ = 43.55 ± 1.96 µm; +/+ *vs* mutants: p>0.5; n = 3-5 ZF/genotype; Mann-Whitney test; ns: non-significant. Values represent the mean ± standard error of the mean (SEM).

Rich media files

Figure 3-video 1: Number of movements of 28 hpf-embryos in their chorion (1 min-video, magnification 0,8x, speed x1) for each genotype: **(A)** *kcnb1*$^{+/+}$, **(B)** *kcnb1*$^{+/-}$ and **(C)** *kcnb1*$^{-/-}$.

Figure 3-video 2: Touch-Evoked Escape Response (TEER) of 48 hpf-embryos (speed x1) showing the trajectory of **(A)** *kcnb1*$^{+/+}$ and **(B)** *kcnb1*$^{-/-}$ conditions.

Figure 4-video 3: Automated tracking of 6 dpf-larvae using the Zebrabox (ViewPoint, France, speed x2)

Figure 1.

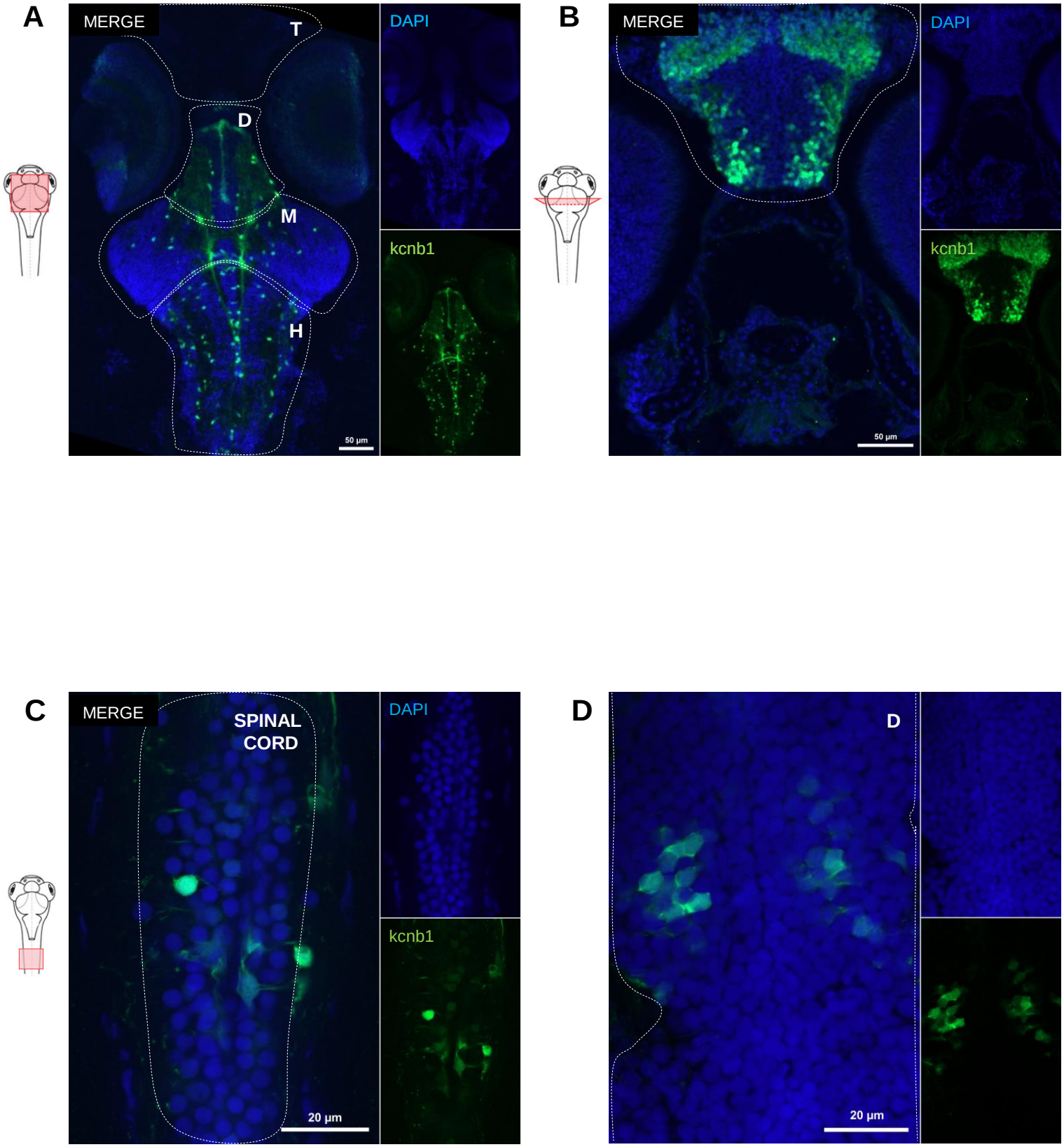
A
MERGE
T
D
M
H
50 µm
DAPI
kcnb1
B
MERGE
50 µm
DAPI
kcnb1
C
MERGE
SPINAL
CORD
20 µm
DAPI
kcnb1
D
D
20 µm

Figure 2.

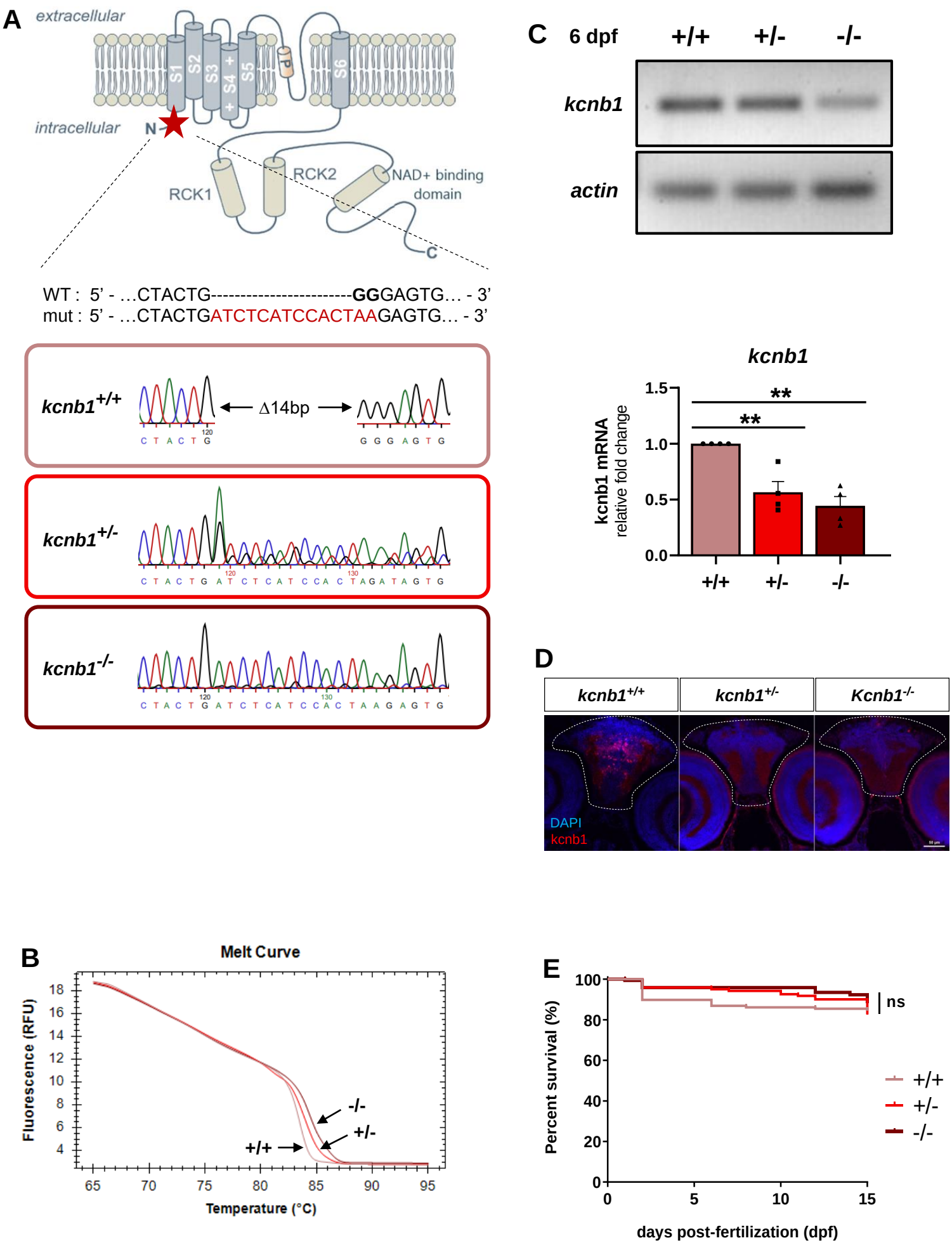
A
extracellular
intracellular
N
C
S1
S2
S3
S4
S5
S6
P
RCK1
RCK2
NAD+ binding domain
WT : 5' - …CTACTG----------GGGAGTG… - 3'
mut : 5' - …CTACTGATCTCATCCACTAAGAGTG… - 3'
kcnb1+/+
Δ14bp
kcnb1+/-
kcnb1-/-
B
Melt Curve
Fluorescence (RFU)
Temperature (°C)
-/-
+/-
+/+
C
6 dpf
+/+
+/-
-/-
kcnb1
actin
kcnb1
kcnb1 mRNA relative fold change
**
**
+/+
+/-
-/-
D
kcnb1+/+
kcnb1+/-
Kcnb1-/-
DAPI
kcnb1
E
Percent survival (%)
ns
+/+
+/-
-/-
days post-fertilization (dpf)

Figure 3.

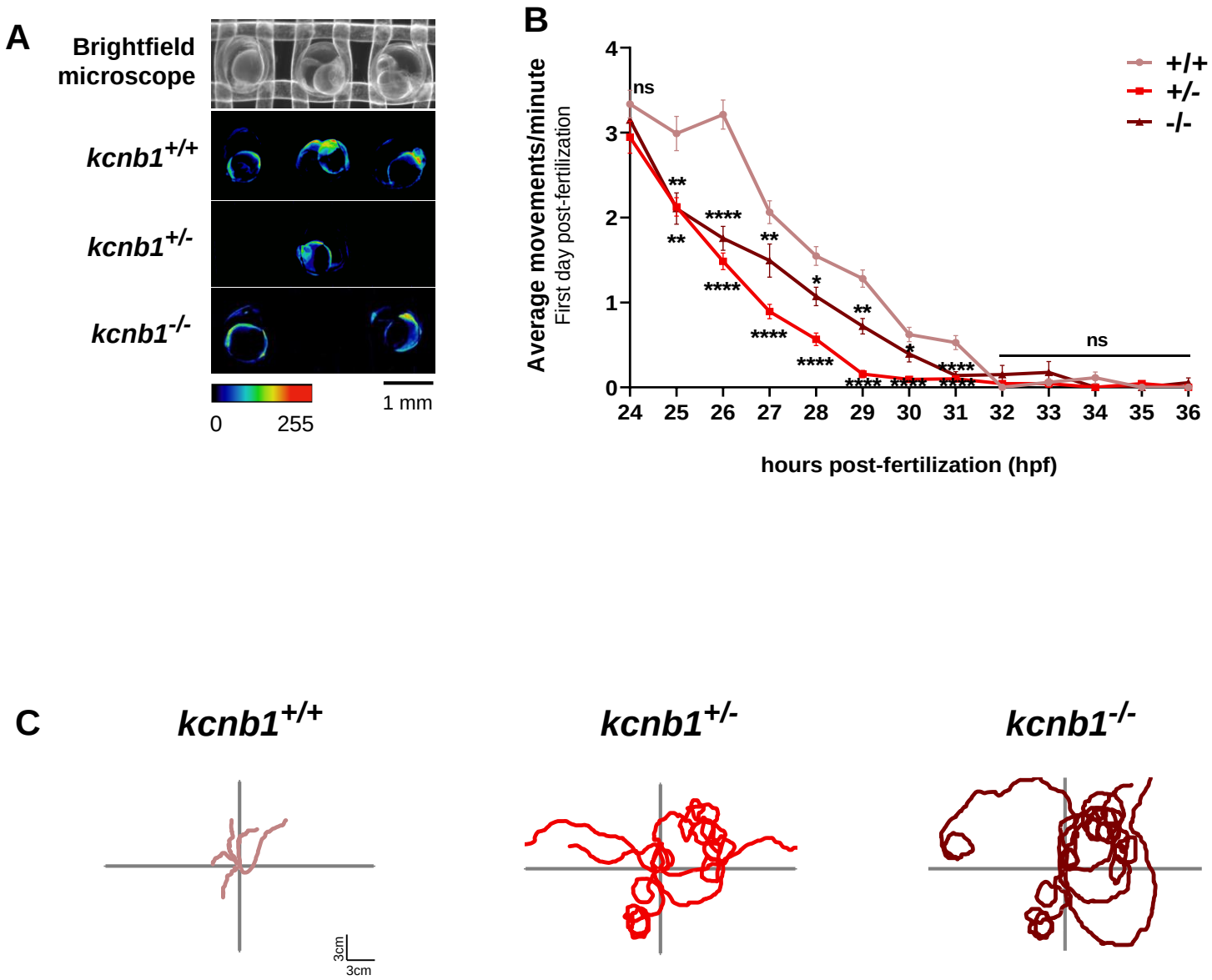
A
Brightfield microscope
kcnb1+/+
kcnb1+/-
kcnb1-/-
0
255
1 mm
B
Average movements/minute
First day post-fertilization
hours post-fertilization (hpf)
+/+
+/-
-/-
ns
C
kcnb1+/+
kcnb1+/-
kcnb1-/-
3cm
3cm
D
Distance swam (mm)
E
Velocity (mm/s)
F
Time spent in motion (s)

Figure 4.

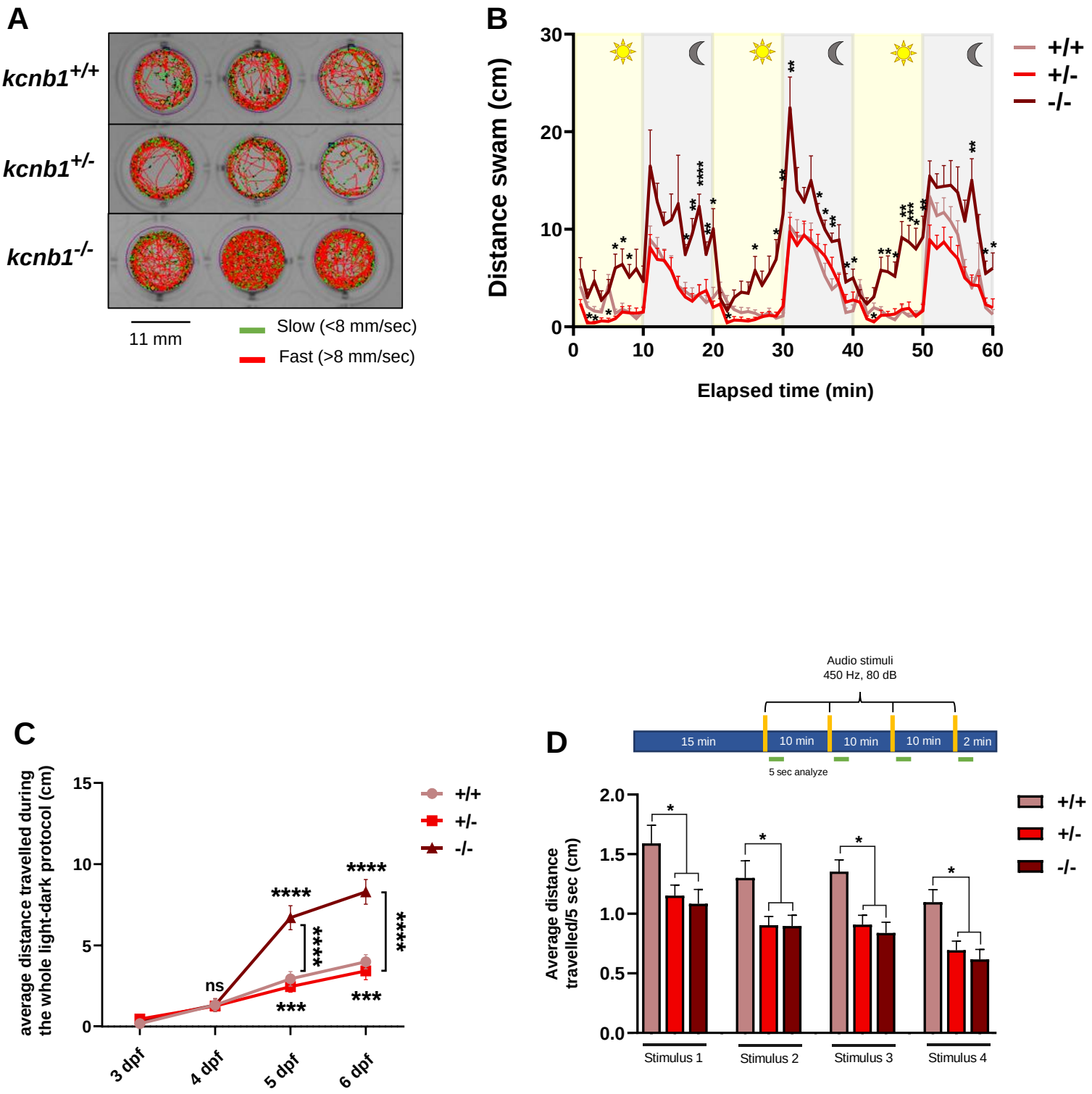
A
kcnb1+/+
kcnb1+/-
kcnb1-/-
11 mm
Slow (<8 mm/sec)
Fast (>8 mm/sec)
B
Distance swam (cm)
Elapsed time (min)
+/+
+/-
-/-
C
average distance travelled during the whole light-dark protocol (cm)
3 dpf
4 dpf
5 dpf
6 dpf
ns
****
***
D
Audio stimuli
450 Hz, 80 dB
15 min
10 min
2 min
5 sec analyze
Average distance travelled/5 sec (cm)
Stimulus 1
Stimulus 2
Stimulus 3
Stimulus 4

Figure 5.

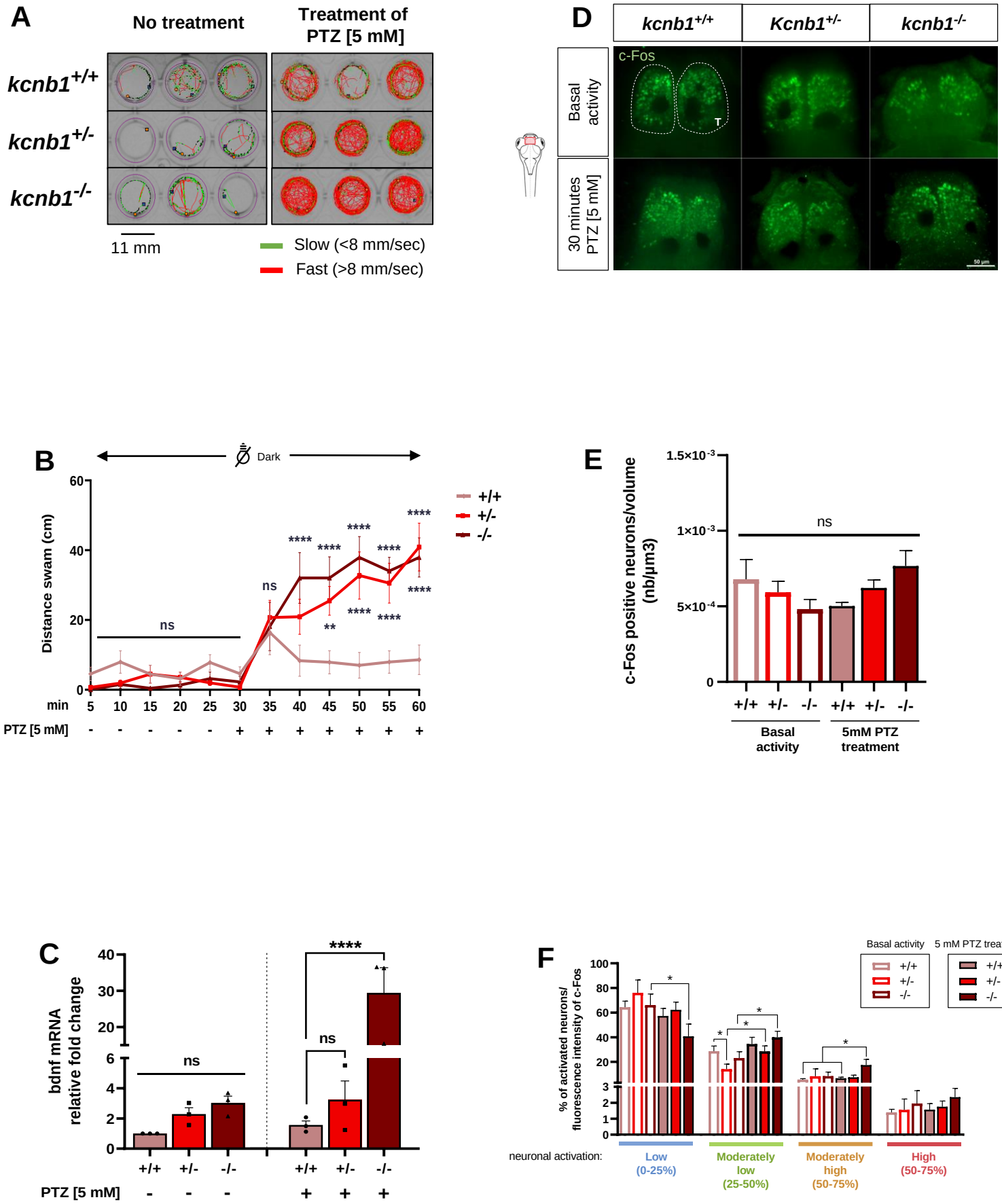
A
No treatment
Treatment of PTZ [5 mM]
kcnb1+/+
kcnb1+/-
kcnb1-/-
11 mm
Slow (<8 mm/sec)
Fast (>8 mm/sec)
D
kcnb1+/+
Kcnb1+/-
kcnb1-/-
Basal activity
30 minutes PTZ [5 mM]
c-Fos
T
B
Dark
Distance swam (cm)
+/+
+/-
-/-
ns
min
PTZ [5 mM]
E
c-Fos positive neurons/volume (nb/µm3)
1.5×10-3
1×10-3
5×10-4
0
ns
Basal activity
5mM PTZ treatment
C
bdnf mRNA relative fold change
PTZ [5 mM]
F
Basal activity
5 mM PTZ treatment
% of activated neurons/ fluorescence intensity of c-Fos
neuronal activation:
Low (0-25%)
Moderately low (25-50%)
Moderately high (50-75%)
High (50-75%)

Figure 6.

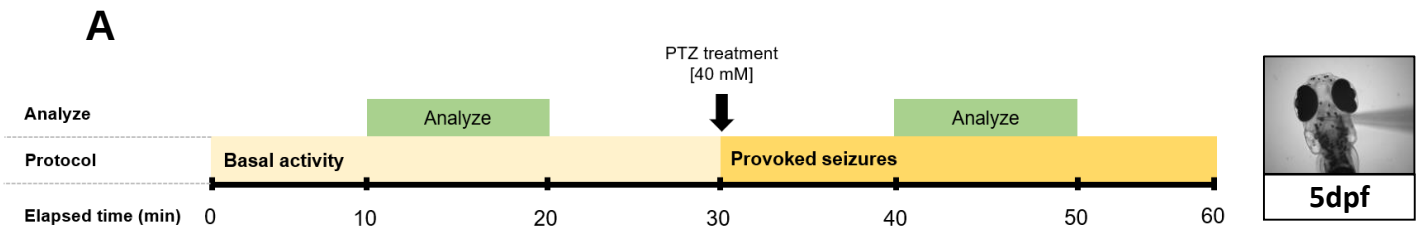
A
PTZ treatment
[40 mM]
Analyze
Analyze
Analyze
Protocol
Basal activity
Provoked seizures
Elapsed time (min)
0
10
20
30
40
50
60
5dpf

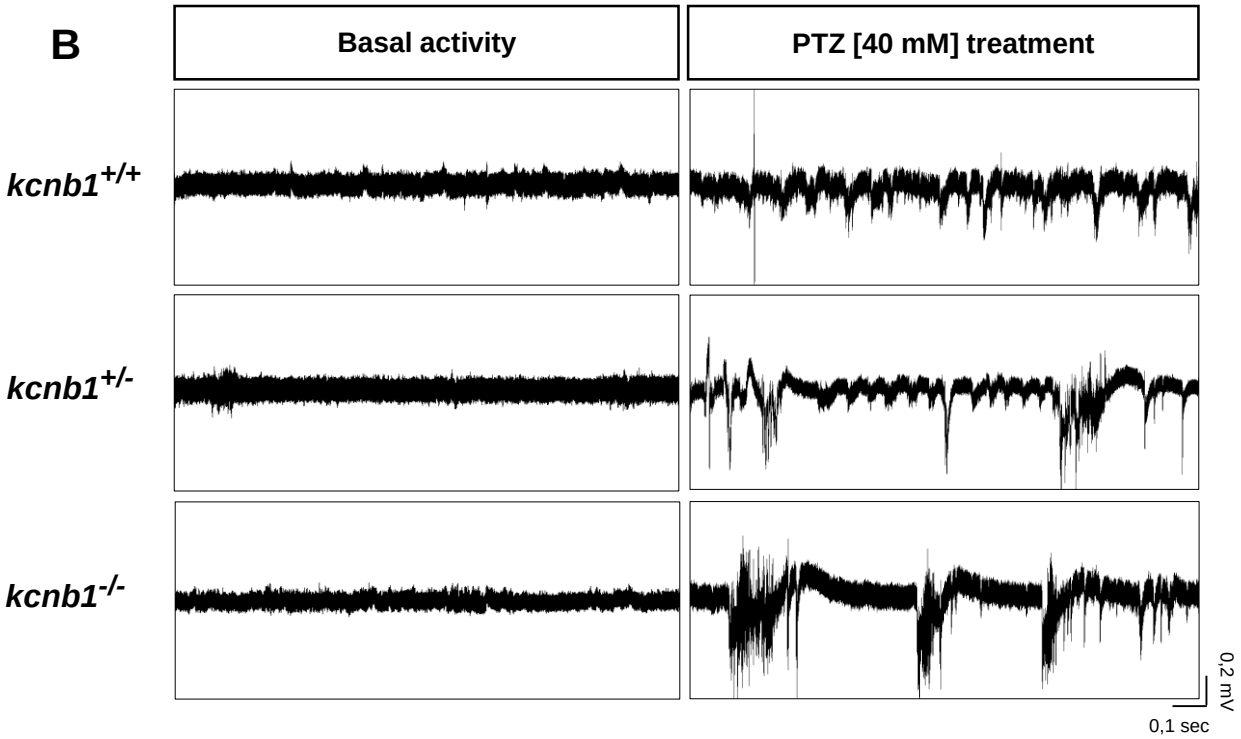
B
Basal activity
PTZ [40 mM] treatment
kcnb1+/+
kcnb1+/-
kcnb1-/-
0,2 mV
0,1 sec

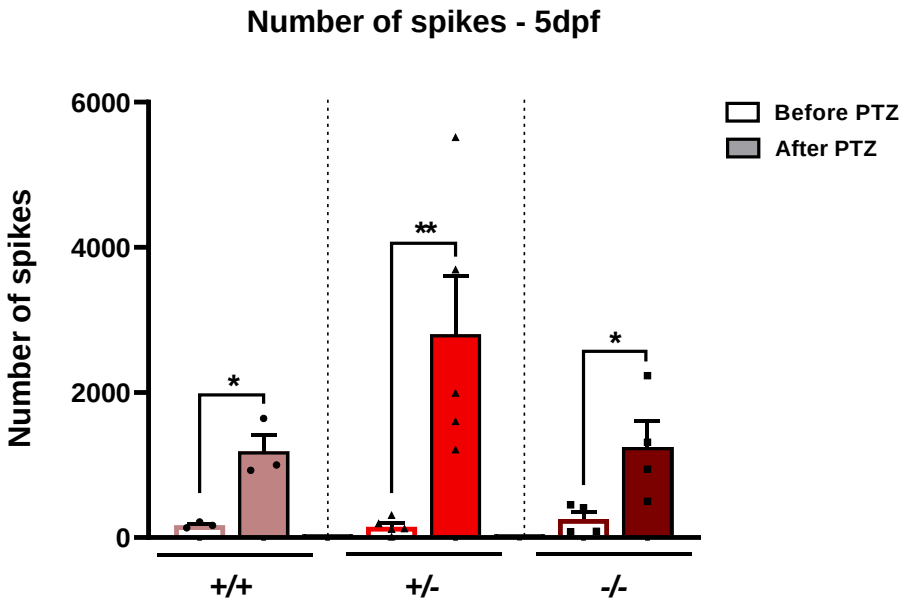
Number of spikes - 5dpf
Number of spikes
6000
4000
2000
0
Before PTZ
After PTZ
*
**
*
+/+
+/-
-/-

Figure 7.

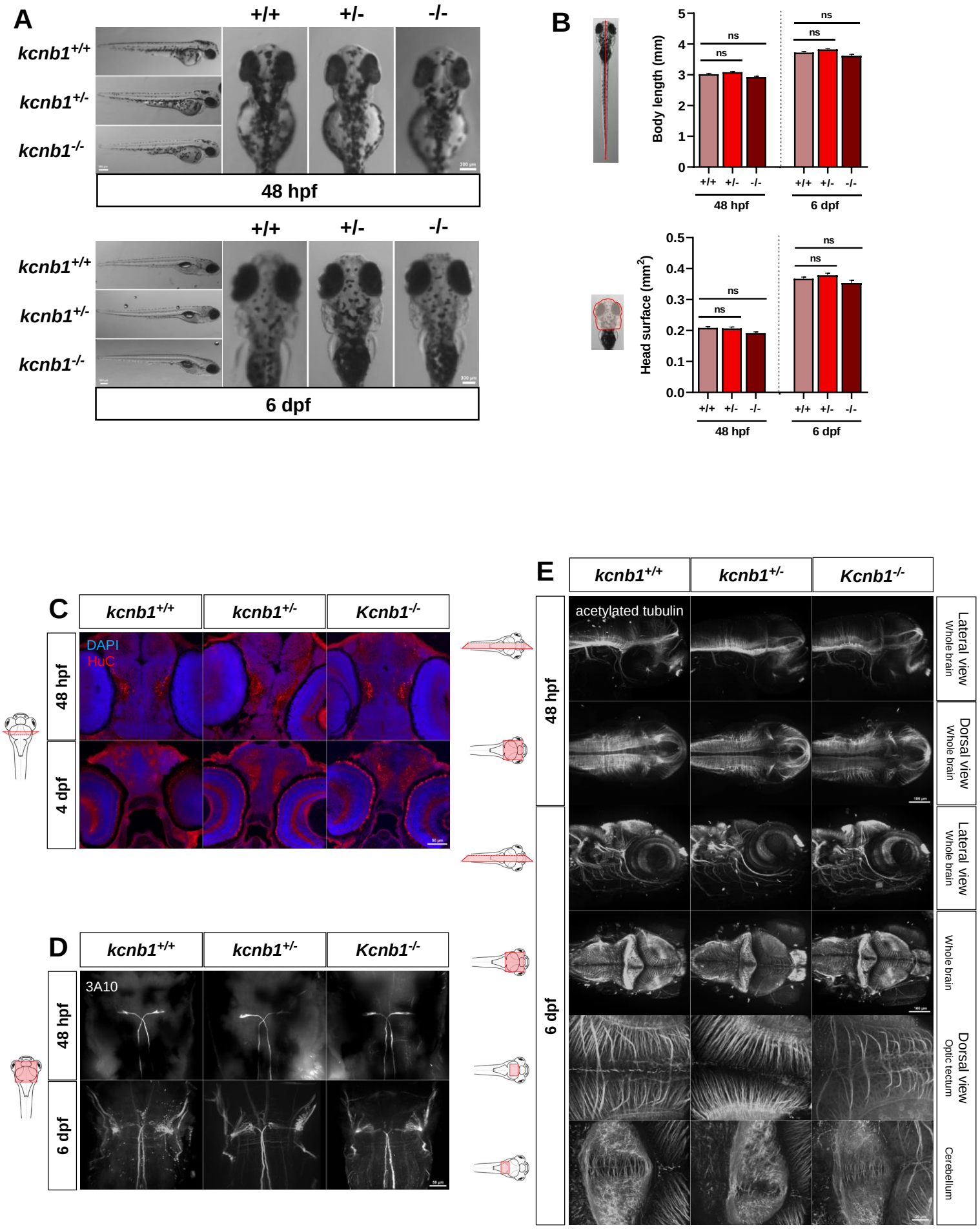
A
+/+
+/-
-/-
kcnb1+/+
kcnb1+/-
kcnb1-/-
48 hpf
6 dpf
B
Body length (mm)
Head surface (mm2)
ns
48 hpf
6 dpf
C
kcnb1+/+
kcnb1+/-
Kcnb1-/-
DAPI
HuC
4 dpf
D
3A10
E
acetylated tubulin
Lateral view
Whole brain
Dorsal view
Optic tectum
Cerebellum

Figure 8.

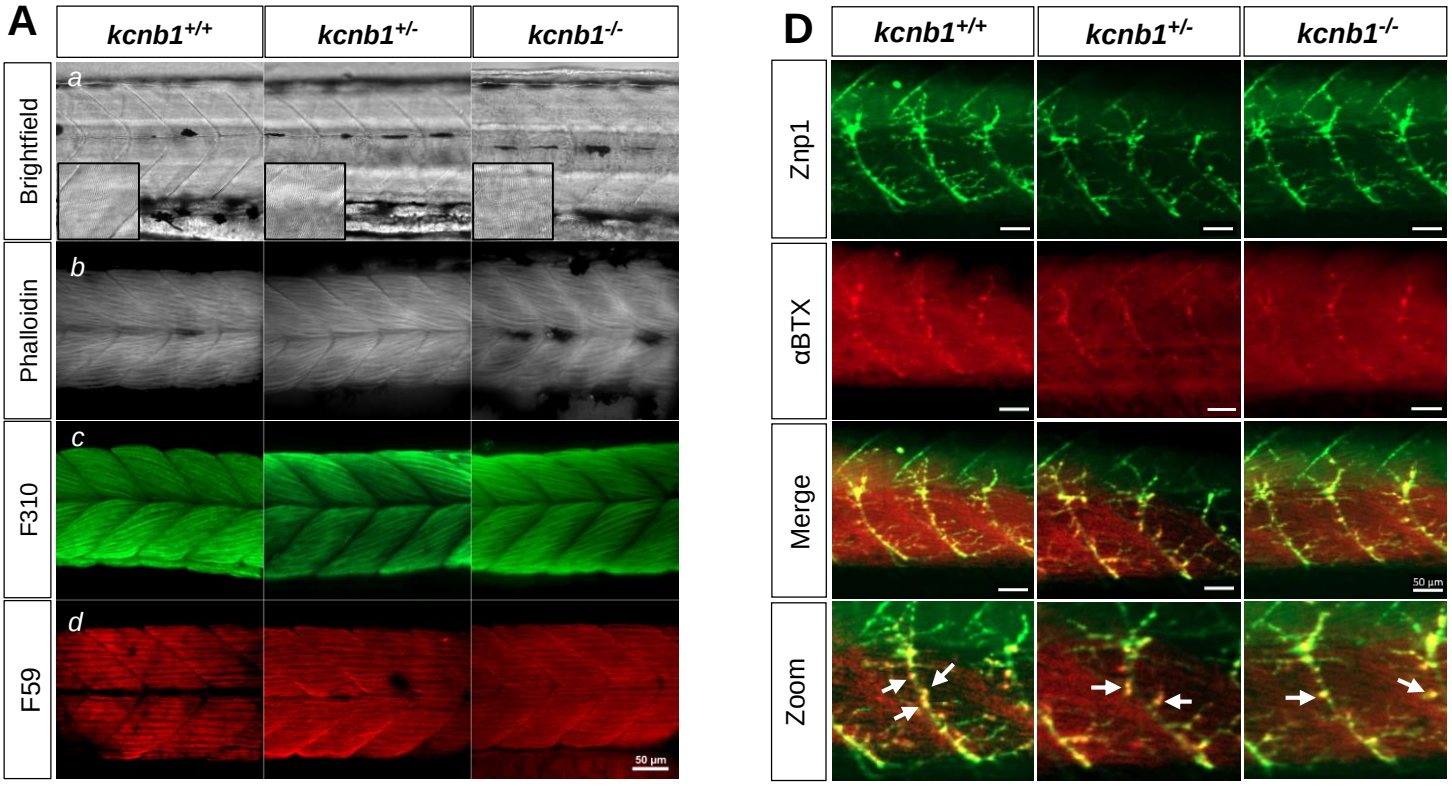
A
kcnb1+/+
kcnb1+/-
kcnb1-/-
Brightfield
Phalloidin
F310
F59
a
b
c
d
50 µm
D
Znp1
αBTX
Merge
Zoom
50 µm

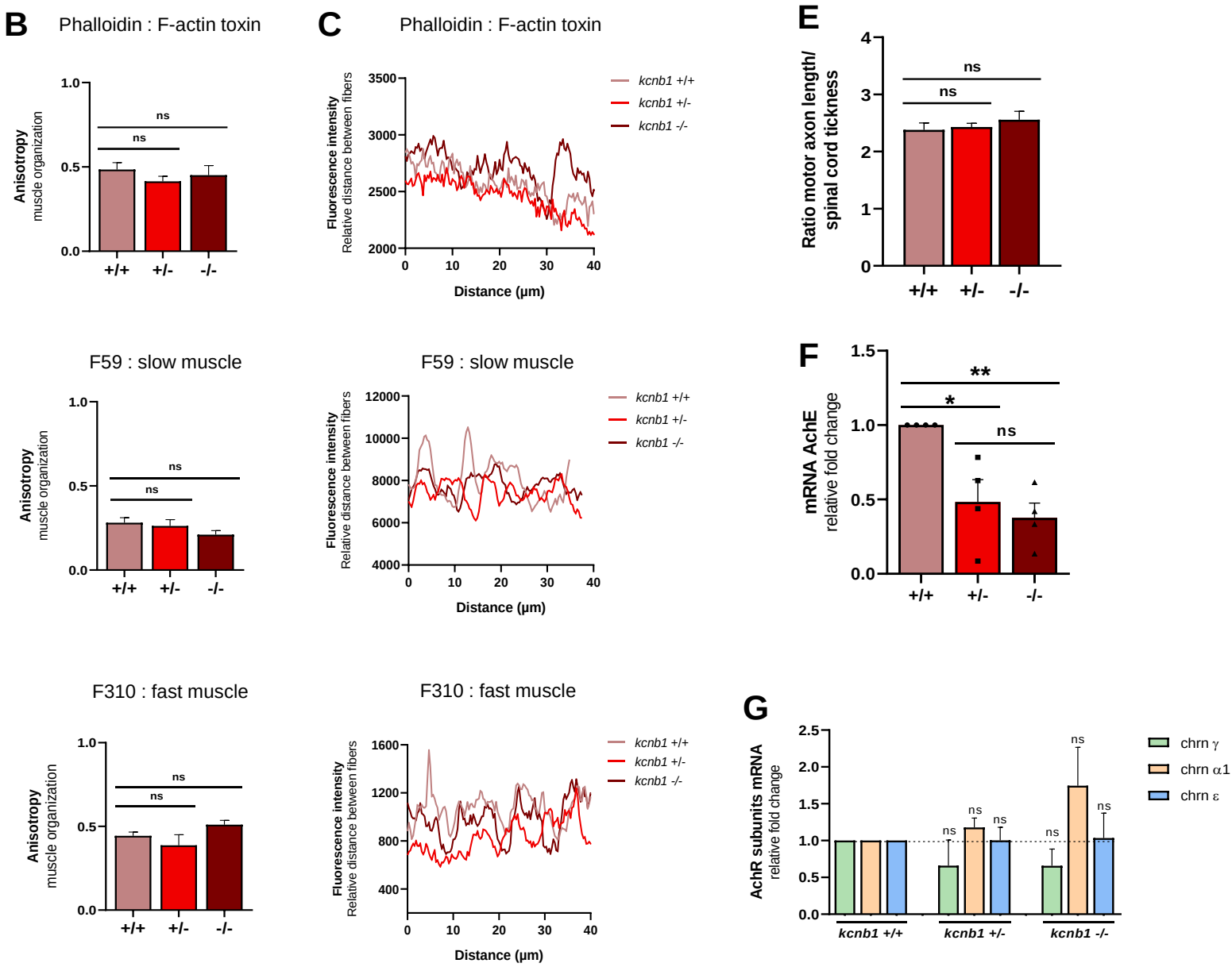
B
Phalloidin : F-actin toxin
Anisotropy
muscle organization
ns
ns
+/+
+/-
-/-
C
Phalloidin : F-actin toxin
Fluorescence intensity
Relative distance between fibers
Distance (µm)
kcnb1 +/+
kcnb1 +/-
kcnb1 -/-
E
Ratio motor axon length/
spinal cord tickness
F59 : slow muscle
F310 : fast muscle
F
mRNA AchE
relative fold change
**
*
G
AchR subunits mRNA
relative fold change
chrn γ
chrn α1
chrn ε

Figure 3-figure supplement 1.

26 hpf	+/+ (n=94)	+/- (n=93)	-/- (n=86)
Coils/min (mean value)	3.212	1.483	1.755

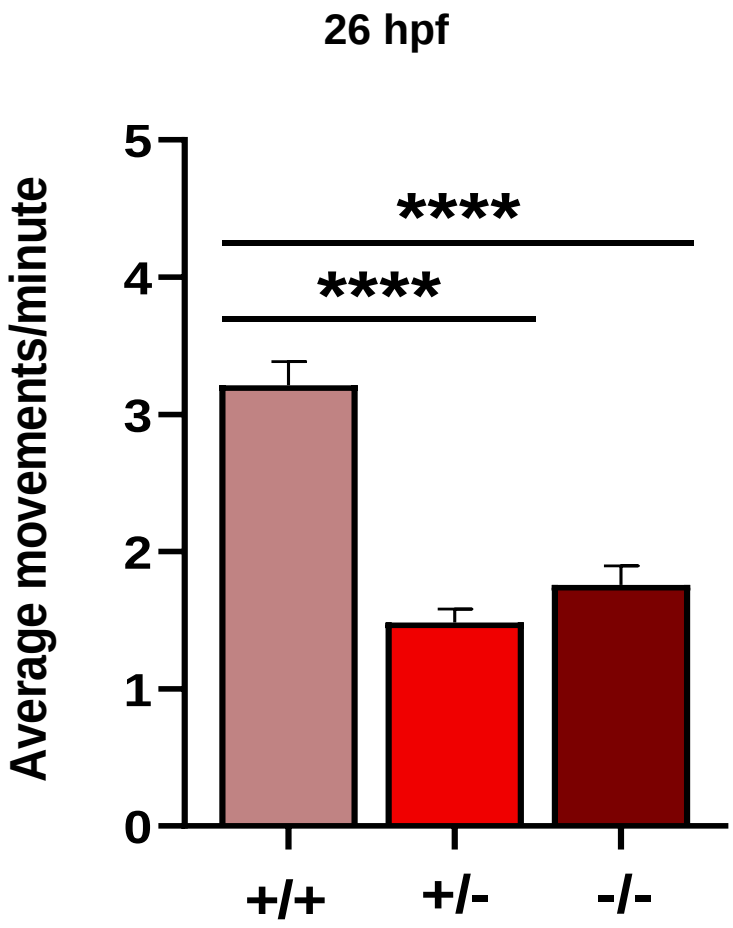

Figure 3-figure supplement 2.

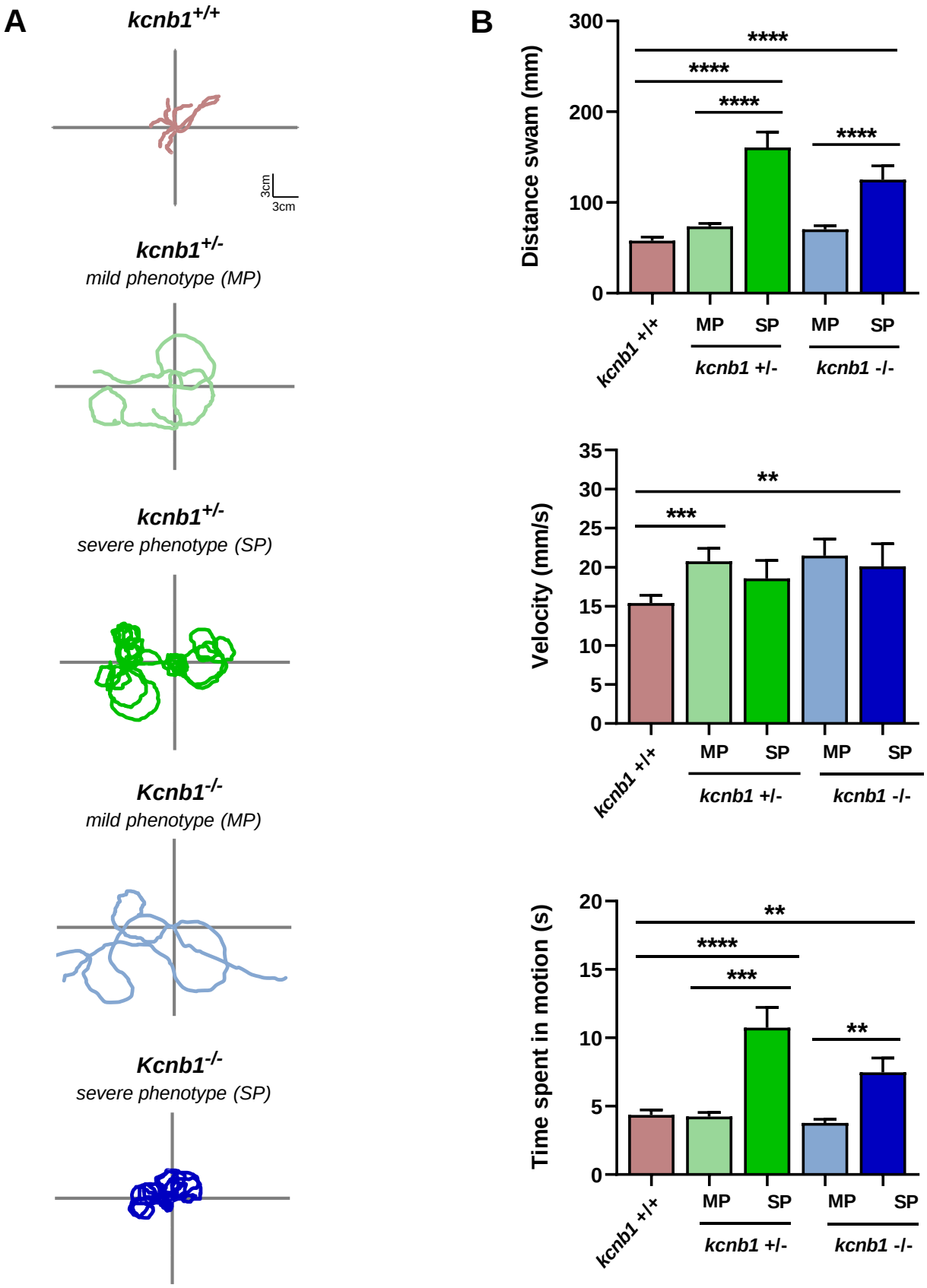

Figure 5-figure supplement 3.

A

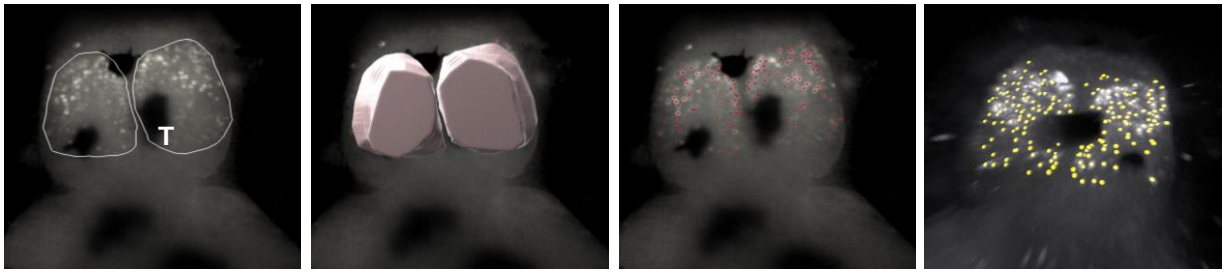

B

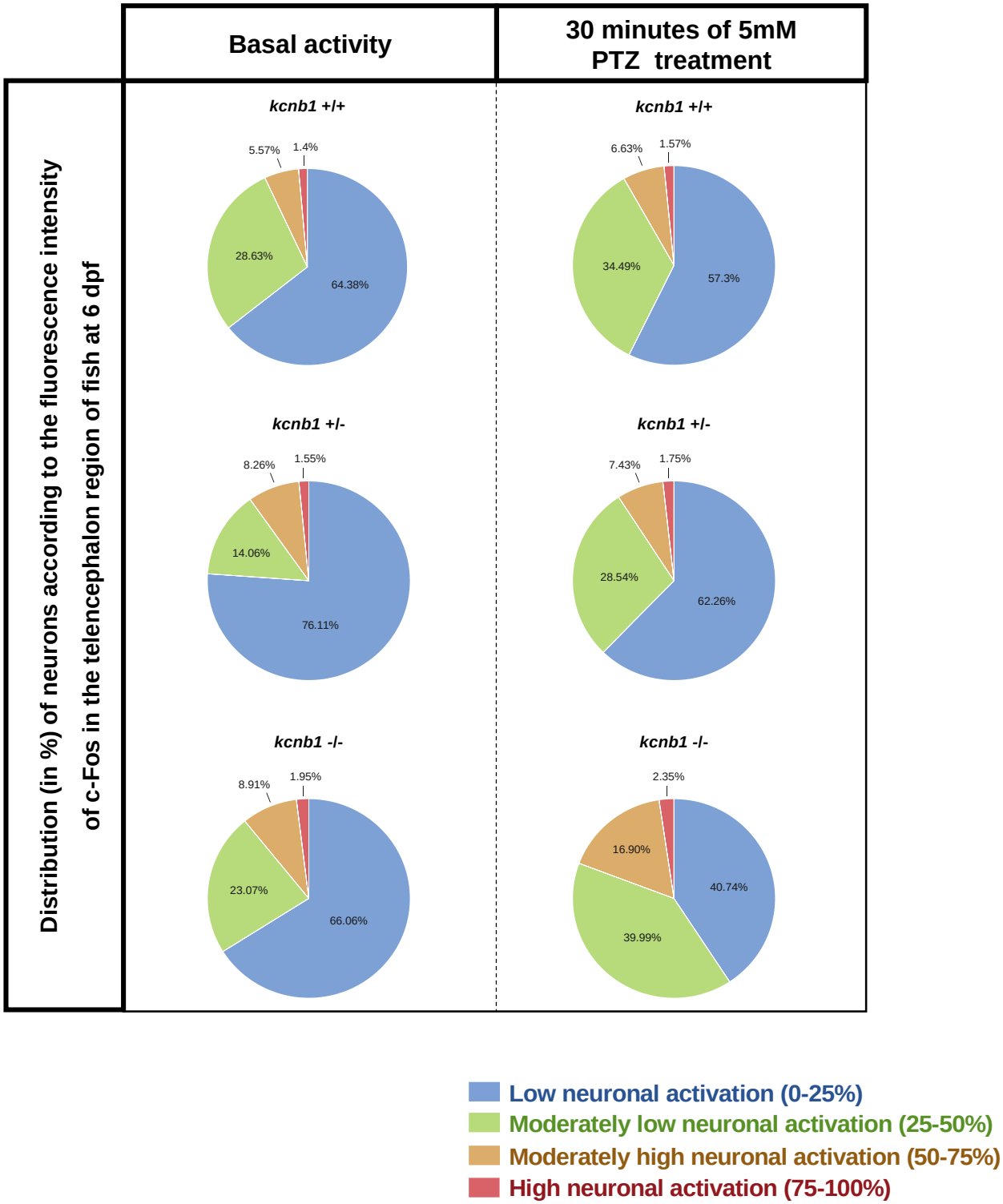

Figure 7-figure supplement 4.

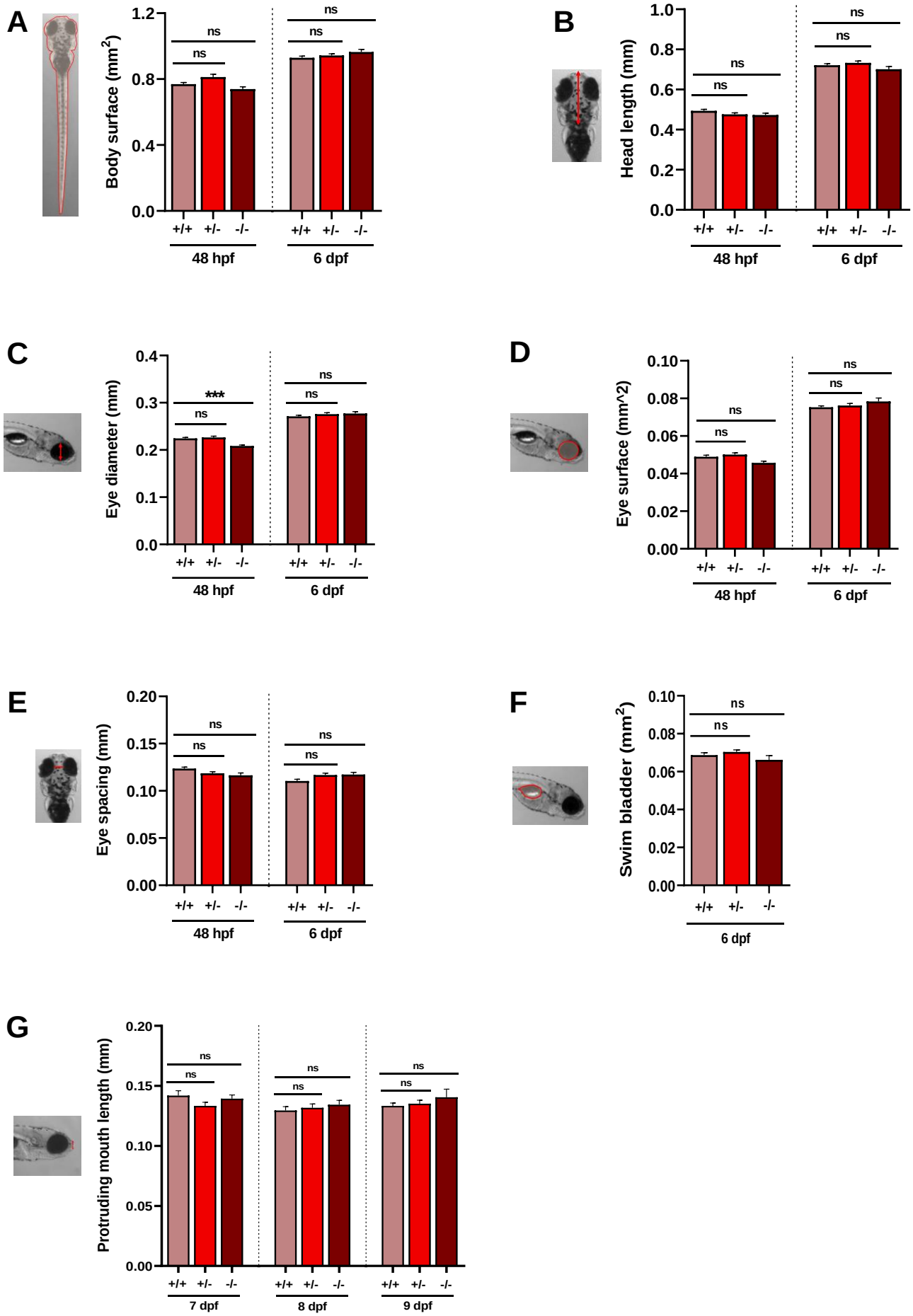
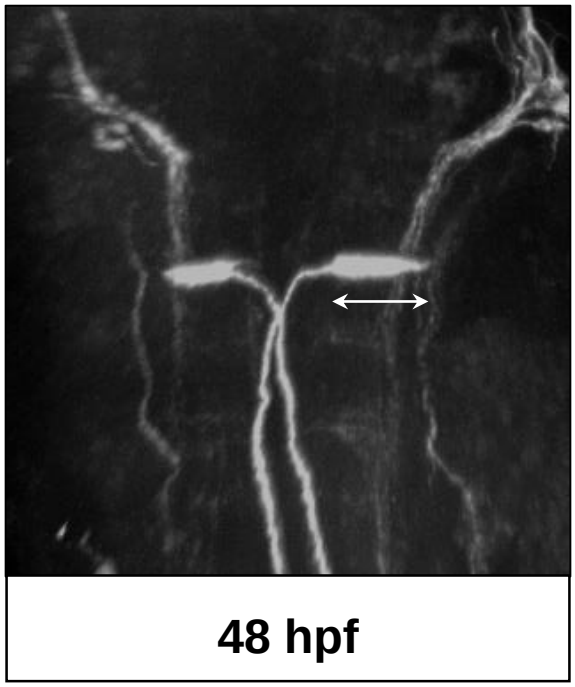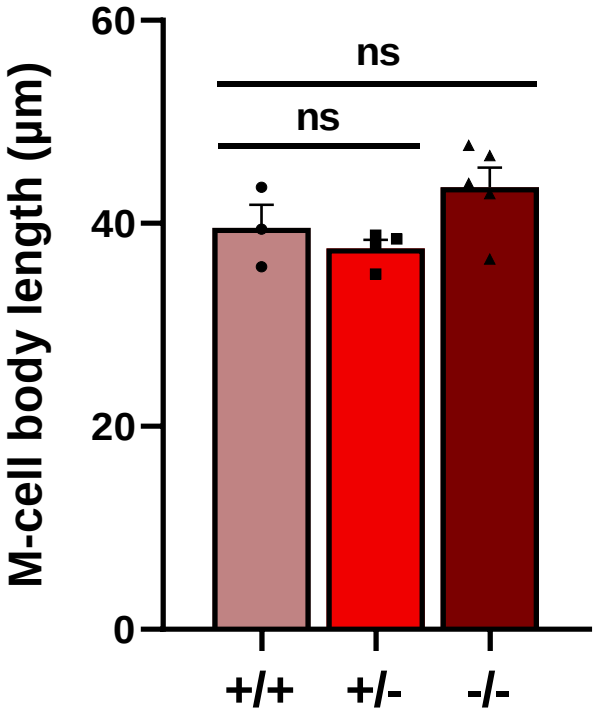
Figure 7-figure supplement 5.